

Problem Description

The overall goal is to determine whether or not distributed Ultra Wideband radars are able to localize and detect fall of a person observed without the person wearing any additional equipment:

- Are the localization methods reliable?
- Accuracy of the methods for positioning. Are the estimates good or correct.
- Are fall detection reliable.

Supervisor: Tor Onshus, ITK, NTNU

Abstract

In a rapidly growing population of elderly people, a system that will allow more of them to stay home for a longer time is of large value to society. A large factor in elderly needing to move from their homes and into caring homes are the risk of injuries from falling. A system that incorporates fall detection will reduce the time it takes for aid to come will therefore be desired. It is also desirable for a system where the person under observation are not required to use any type of sensory equipment. This thesis explore the use of distributed radars for the purpose of fall detection without wearable sensors.

In this thesis it will be presented methods for range estimating using returned reflections from the environment with the use of Ultra Wideband Radars and how to use these estimates for target localization. Through the use of weighted least square and nonlinear least square method, positions of objects are estimated in three dimensions. The problems of bias in the range estimates from the body not being a point are analyzed and the relation between radar placement and object position are also discussed. Lastly, the thesis presents a method for fall detection through determinate whether a person is lying on the floor over a time period.

Sammendrag

I en raskt voksende befolkning av eldre, er et system som gjør at flere av dem har mulighet til bli hjemme lengre av stor verdi for samfunnet. En stor faktor i at eldre må flytte fra hjemmene sine og inn i omsorgsboliger er risikoen for fallskader. Et system som inkorporerer fall deteksjon vil redusere tiden det tar før hjelp kommer og vil derfor være ønskelig. Det er også ønskelig for et system hvor personen under observasjon ikke er pålagt å bruke noen form for sensorisk utstyr. Denne oppgaven undersøker bruken av distribuerte radarer for det formål detektere fall uten at brukeren trenger å ha på seg noe utstyr.

I denne masteroppgaven vil det bli presentert metoder for posisjon estimering ved bruk av Ultra Wideband radarer. Gjennom bruk av metoder brukt i GPS for posisjonering, blir posisjonen beregnet i tre dimensjoner. Problemene som oppstår ved at kroppen har en ytre grense og at det er denne grensen som blir målt av radarane blir analysert. Forholdet mellom radar plassering og objektplasseringen blir også diskutert. Til slutt, presenterer avhandlingen en metode for fall deteksjon gjennom å avgjøre om en person er liggende på gulvet over en tidsperiode.

Contents

Problem Description	i
Abstract	iii
1. Introduction	1
1.1. Motivation	1
1.2. Concept	1
1.3. Thesis Outline	2
1.4. Other Technologies	3
2. Range Estimation	5
2.1. Radar Signal	5
2.2. Cluttermapping	6
2.3. Pulse Signature Matching	8
3. Position Determination	9
3.1. Trilateration	9
3.2. Nonlinear Least Square Method	12
3.2.1. Finding a good initial estimate	14
3.3. Human Movement Model	16
3.4. The Kalman Filter	17
3.5. Radar Placements	19
4. Testing	21
4.1. Setup	21
4.2. Test Scenarios	22
5. Simulation	27
5.1. Point Object Simulation	27
5.1.1. Zero Noise	28
5.1.2. Noise Scenario	30
5.2. Spherical Object Simulation	32
5.2.1. 3 Radars	33
5.2.2. 4 Radars	34
6. Fall Detection	39
6.1. Height Based Fall Detection	39

7. Discussion	43
7.1. Ranging	43
7.2. Localization and Tracking	43
7.3. Fall Detection	44
8. Conclusion	45
9. Future Work	47
Bibliography	49
List of Figures	53
A. On the CD	55
B. System and Hardware	57

1. Introduction

The topic of this project is fall detection using ultra wide-band (UWB) radars and signal processing algorithms. This chapter will give a brief background to this research field and some of the applications that uses ranging and human detection. The possibility to determine if a fall have occurred can help inn cost reduction and safety of elderly people.

1.1. Motivation

The motivation for this master thesis is to be able to create a fall detection system to be used in a safety-at-home system for elderly living alone. In Norway alone, it is estimated that more than 200 000 elderly people fall in their home each year. Of these, about 50% can't get up again on their own and is in need of assistance, and about 40-60% need medical treatment [1]. The faster aid arrives at location, the better the prognosis for a recovery to same level of health and movement as the patient had before the fall. The commercial available aids and equipment on the market are wearable sensors or alarms that requires the person using it to be of consciousness or are simply not accurate enough to be reliable [2]. Since the equipment also often is needed to be on the user, there are chances of forgetting to put them on in cases of dementia or simply small tasks that are not deemed to strenuous to take on the equipment, but the user still falls and can't get up, as in a case of nightly visit to the bathroom and the user is in a rush to get out of bed and onto the toilet. By using radars as sensors to using only information regarding the distance to the user, the user don't need to think about wearing anything and 'feel old' by having to wear equipment. A complete system should be able to reliably detect fall, and send a message to medical personnel with instructions to come to the aid of the patient.

1.2. Concept

The concept for this approach of fall detection is a passive solution, meaning the user should not need to wear any equipment or be active in the detection in any way. In the event of an accident where the person falls or simply becomes incapacitated, an alarm should go off at the appropriate monitoring personnel system.

A person might not like to have the necessary equipment from the other detection schemes on them, or they simply might forget to put it on. To avoid this, a sensor scheme where the person observed is the measurement, and not a reference sensor. To do this, monostatic UWB radars are chosen as the sensor.

A monostatic UWB radar works by sending out an electromagnetic pulse that travels at the speed of light, and wait for it to be reflected back. By measuring the time between the radar sends its pulse and the reflections comes back, one can calculate the distance traveled by the pulse. The distance to the reflecting object is then half the time between sending and receiving times the velocity of the pulse.

By placing multiple radars in the environment, one can acquire a range measurement from each radar. Then Triangulation and position estimation schemes that use these distance measurements are applied together to estimate the position of the person in 2D or 3D space. By the use of these methods one can estimate the height and position of a person in a room.

One can use the estimated height to decide whether a person is standing or lying on the floor.

1.3. Thesis Outline

The thesis will be presented in a sequential manner to give the reader an understanding of the basic building blocks the process of fall detection will depend on. Fig. 1.1 shows the information/data flow behind this thesis idea for fall detection. The thesis will be constructed in such a way that, first, a brief explanation of how the radars gathers a range estimate from the environment is presented in chapter 2. This part will for the most consist of the work done in the project thesis [3] from fall 2013, and some new ideas to avoid disturbances in the measurements.

In chapter 3 we will introduce some of the theory and math behind Trilateration and GPS positioning. A human movement model to use with the Kalman Filter is then proposed. By using the Kalman Filter, one can use the estimated position vector as input and get the a new estimated position, velocity and acceleration. Collectively we call this states.

In chapter 4, we present the results after testing the system on pre-scripted fall scenarios conducted. To overcome the physical limitations that restricted the testing, simulations of different movement scenario were conducted in chapter 5. In chapter 6 we use the estimation $\hat{\mathbf{x}}$ of the position vector $\mathbf{x} = [x, y, z]^T$ to propose an algorithm to determine whether or not a person is standing or lying on the floor

In chapter 7 we have general discussion on the findings of this thesis and in chapter 8 we present our concluding remarks. Finally, in chapter 9 we briefly discuss further work.

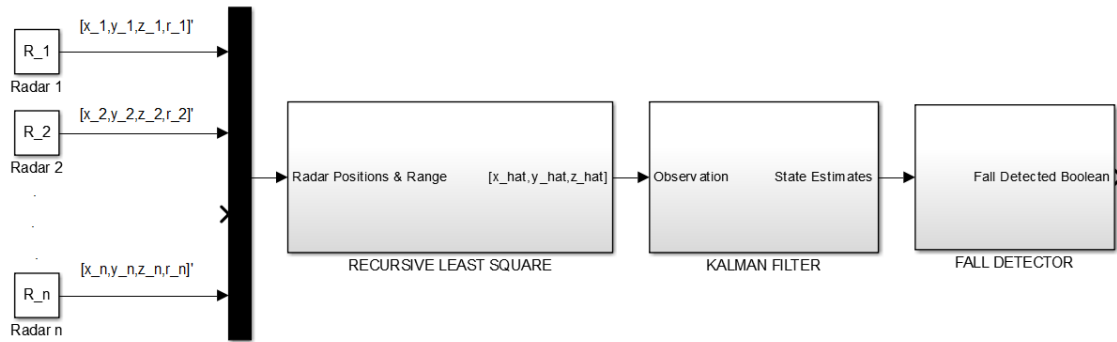


Figure 1.1.: Data Flow

1.4. Other Technologies

Audio Based Detection

Litvak et al. [4], proposes a system that detects falls by sound and floor vibrations. It uses non-wearable devices, thus overcoming the drawback of people forgetting to wear the sensors. Accelerometer used to detect vibrations of the floor, and microphones are placed in a corner of the room, and falls are detected using an energy-based event detection algorithm. The event is classified to between human falls and falls of objects using pattern recognition algorithms. The system have a 95% specificity and sensitivity when tested with a human like doll. Specificity means that 95% of the falls were detected, and sensitivity meaning that 95% of the detected falls were true falls.

Accelerometer

Bourke et al. [5] proposes a detection system using a waist mounted tri-axial accelerometer for detection. Using a an algorithm that employs thresholds in velocity, impact and posture, the system achieves 100% specificity and sensitivity with a false-positive rate of less than 1 false-positive per day of waking hours. The method is reliant on the person wearing the accelerometer.

Camera Based Detection

Anderson et al. [6], proposes a camera based system using a segmentation method based on color to recognize the silhouette of a person. When the silhouettes are obtained, features are extracted and using a hidden Markov model to recognize different activities. Based on the classification from the hidden Markov model fall can be detected. The article don't mention the sensitivity or specificity of the method.

2. Range Estimation

This chapter will give a brief review of the range estimation schemes that were worked out in the Project Thesis from fall 2013 [3]. We also address some of the problems that arose and some expanded methods used to solve them. The first section will give an introduction to how the signal from the radar looks and how the 'echo/reflection' is stored and presented in 'frames'. The next section will present the method used to remove static reflection, also known as 'clutter'. When the signal is clutter free, it can be used to find signals of interests. To either look for reflections that indicates movement or simply new objects that have entered the radars field of observation. Lastly, the method for locating the signal of interest and estimate the range is presented in sec. 2.3.

2.1. Radar Signal

The Novelda NVA-R641 UWB radar generates a pulse by using a wide specter of frequencies, usually in the 0.85-9.55 GHz range. An illustration of the pulse is shown in Fig. 2.1. It is sent outward in the area of observation. The observed area is restricted by the azimuth of the antennas main lobes in horizontal and vertical directions. As the pulse propagates outwards, the energy of the signal weakens. The signal that is reflected needs to travel the same distance back, and the same attenuation of power occurs. Ghassemzadeh et al. [7] describes the energy at a given distance is given by

$$P(r) = P_0 - 10 \log_{10}(r/r_0) \quad (2.1)$$

The radar uses a hold-and-sample digital sampling scheme. The sampling window is in the nanoseconds range. The sum of the incoming signal value captured in this time is stored as a sample point in a vector called 'frame'. We can then calculate range by multiplying the speed of light with the sampling time. Thus, for each sample point one can distinguish between distances down to 4mm. With a total of 512 sample points in a frame, we get an observation sector close to 2m in radius for each frame. We can also choose a Frame Offset, a time delay the radar waits before it starts sampling. By setting a Frame Offset, the inner radius of an annulus is determined. and we get the sector of observation by choosing

$$V = \int_0^\phi \int_0^\theta \int_{r_{FO}}^{r_{FS}} r^2 \sin(\theta) dr d\theta d\phi = \frac{1}{3}(r_{FO}^3 - r_{FS}^3)\phi \cos(\phi) - \sin(\phi). \quad (2.2)$$

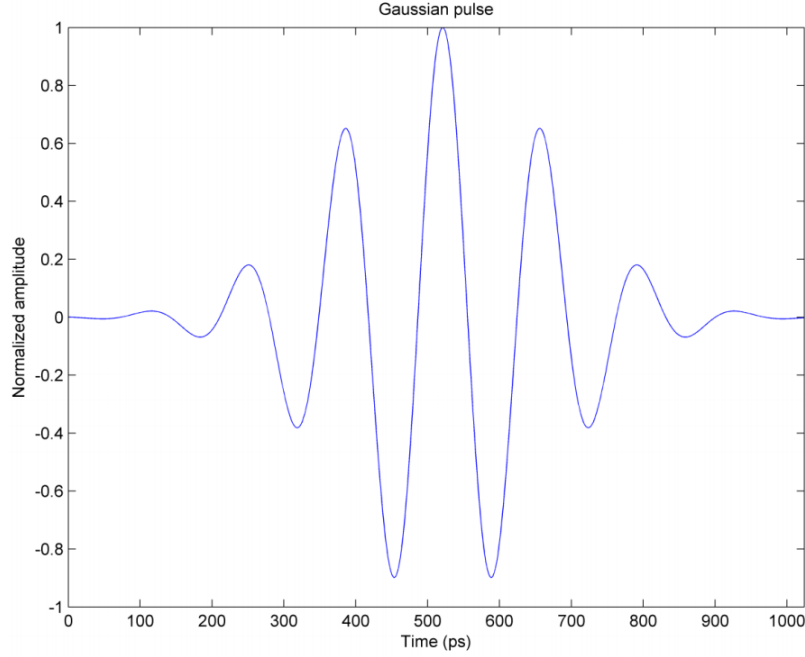


Figure 2.1.: UWB Pulse Signal

V is the radars observation volume, where ϕ and θ is the spreading of the antenna in horizontal and vertical direction respectively. r_{FO} and r_{FO+F} are the ranges set by the Frame Offset and the length of a frame pluss the frame offset respectively. The radar can stitch together several frames to generate a larger observation area. A typical frame may look like Fig. 2.2.

2.2. Cluttermapping

When a person moves in a room observed by the radar, we need to separate the reflections from the person from the reflections from the environment. We call this process for Cluttermapping. Cluttermapping is remembering the reflections from a static environment. By removing these static reflections, it becomes easier to locate signals of interests. This is done in two different ways. We can either observe new objects, or movement in the area. The two schemes are called Static Direct Mean and Adaptive Direct Mean respectively. Both of these methods are explained in the following sections.

Static Direct Mean

We begin with a clear observation area, i.e. a room with nobody in it. We then take N frames, detecting the signal from walls and furniture. By storing the N

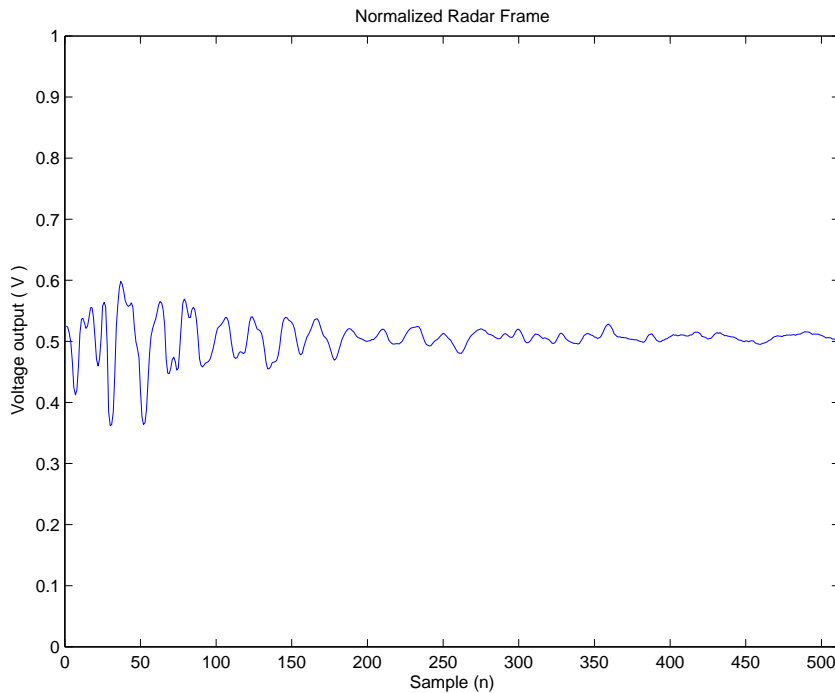


Figure 2.2.: Normalized radar signal represented as a frame.

frames of an empty observation area, one can create the simple static cluttermap. By averaging the N samples to reduce noise, we have a good approximation of the static environments reflections. When subtracting the static cluttermap from the radar frame, it shows all new objects that have entered the observation area. The strength of this cluttermap is that the objects that entered the area do not 'vanish' after a while, but the signal reflection amplitude it gives off is the same. On the other hand, the weakness is that it is very susceptible to change in the environment, e.g. a chair moved from its original placement.

Adaptive Direct Mean

Unlike the static cluttermap mentioned above where we store N frames of a known empty area, the adaptive method uses the N **last** frames. By taking the mean and subtracting it from the very latest captured radar frame, moving objects will become the only remaining reflection. This approach makes recent movement 'fade' into the static background. Thus, a dynamic environment such as a living room, where chairs and furniture often are moved a bit around, will gradually become a part of the cluttermap. A disadvantage to the adaptive cluttermapping is that it is quite susceptible to noise. A short window is similar to using the derivative of the signal, thus enhancing noise. It is also possible to experience an image shadow, as object placed between a wall and a radar when moved after being stationary for a while, will generate a new reflection on the wall as well as in the place where it was

placed since there are new reflections coming of it.

2.3. Pulse Signature Matching

Pulse Matching is the basis for estimating the range. A reflection template is generated by placing the desired object of detection in front of the radar and subtracting the static cluttermap. By using the template of the desired object, a cross correlation between the processed radar frame and the template can be done. By finding the sample point n_{max} , within the frame that gives the highest value from cross correlation with the template, one can then calculate the range by multiplying the window time frame with the speed of light. This gives us the range

$$r = c\tau n \quad (2.3)$$

where c is the speed of light, τ is the time a sampler uses to measure incoming reflections and n is the sample number. The sample number used for output is n_{max} . A presentation of the resulting signals after cluttermapping, cross correlation and range determination can be seen in Fig. 2.3.

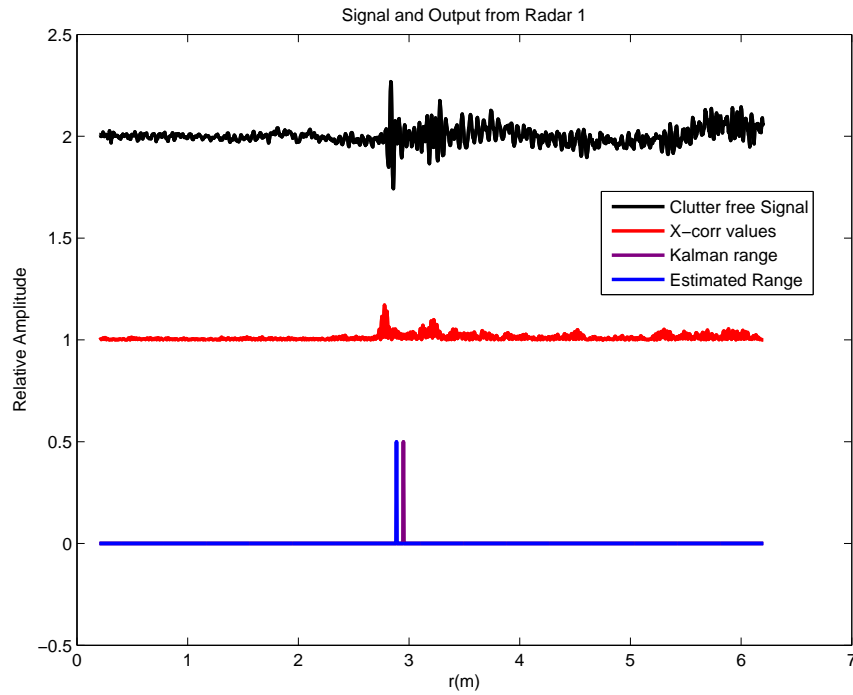


Figure 2.3.: The signals and values generated by range estimation. Signals have been scaled down and shifted for viewing.

3. Position Determination

This chapter introduces methods used for localization and tracking by position determination. A common method used for localization of a specific source given distance measurements by the use of Trilateration are derived. The challenges that arise when the source is no longer a point are presented. Furthermore, a Nonlinear Least Square (NLS) method are also derived with inspiration from the principles behind Global Positioning System (GPS). The initial estimate problem of the NLS are also resolved. A model for human movement is then presented and will be used as the basis for the Kalman filter that also is introduced. Lastly, we discuss optimal radar placement. The initial estimate problem and radar placement are based on the framework presented in the Project Thesis of Jørgensen,[8].

3.1. Trilateration

Trilateration is an often used method in navigation and position determination [9, 10, 11, 12, 13]. The method finds the position of the object by the use of range estimates and radar positions. In two dimensions one only needs two radar positions and two range estimates to generate a unique position in a room, as long as the radars are placed along a wall. As you add an additional dimension to the desired position estimate, one will need at least three positions and range estimates. The range estimates can be expressed as equations for spheres such as

$$r_i^2 = (x - x_{r_i})^2 + (y - y_{r_i})^2 + (z - z_{r_i})^2 . \quad (3.1)$$

We start with the three spheres, and set the origin of the reference frame in the center of one of the radars. We then place the second radar in such a way that it lies on the xy -plane a distance d from the first radar on the x -axis and its coordinate placement is $(d, 0, 0)$. The third radar is placed at location $(i, j, 0)$. The spheres will then intersect as shown in Fig. 3.1.

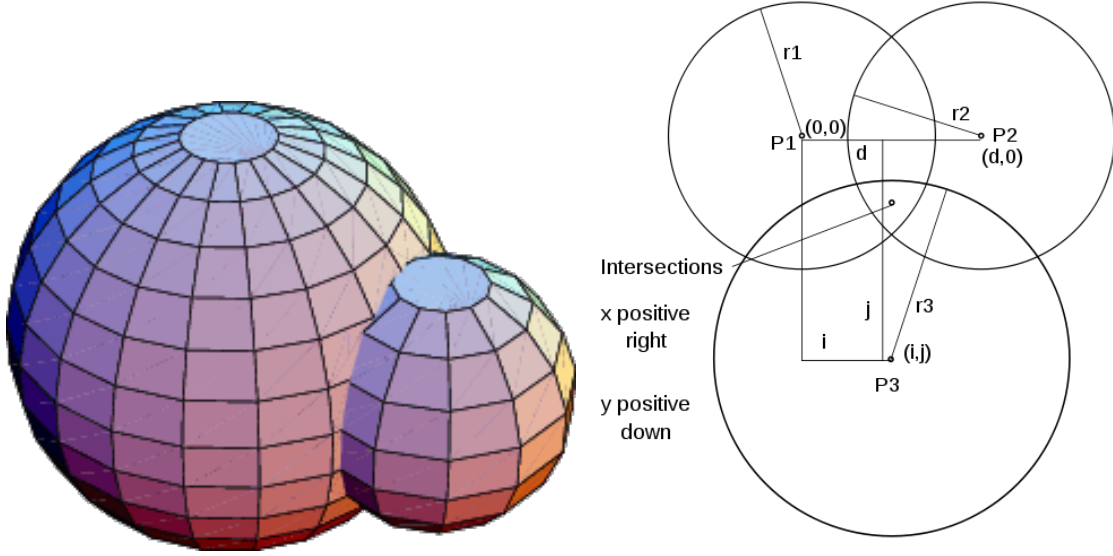


Figure 3.1.: Sphere-Sphere Intersection. Image taken from [11] and [14]

Knowing the positions of the radars, equation (3.1) now becomes;

$$r_1^2 = x^2 + y^2 + z^2, \quad (3.2)$$

$$r_2^2 = (x - d)^2 + y^2 + z^2, \quad (3.3)$$

$$r_3^2 = (x - i)^2 + (y - j)^2 + z^2. \quad (3.4)$$

By rearranging (3.2) and inserting it into (3.3) and solve for x , we get

$$x = \frac{d^2 - r_2^2 + r_1^2}{2d}. \quad (3.5)$$

This is an equation for a circle with center in $(x,0,0)$ with radius $\sqrt{r_1^2 - x^2}$. This circle is the intersecting points of the two spheres. By utilizing the third equation in the same manner and solve for z^2 in (3.2) and substituting it into (3.4) we have

$$y = \frac{r_1^2 - r_3^2 + i^2 + j^2}{2j} - \frac{i}{j}x, \quad (3.6)$$

and finally, by substituting (3.6) back into (3.2), we get z

$$z = \pm \sqrt{r_1^2 - x^2 - y^2}$$

$$= \pm \sqrt{r_1^2 - \left(\frac{d^2 - r_2^2 + r_1^2}{2d} \right)^2 - \left(\frac{r_1^2 - r_3^2 + i^2 + j^2}{2j} - \frac{i}{j} \left(\frac{d^2 - r_2^2 + r_1^2}{2d} \right) \right)^2}. \quad (3.7)$$

Depending on the ranges, the real part of z can have two, one or zero solutions. The different outcomes of z can be illustrated in Fig. 3.2.

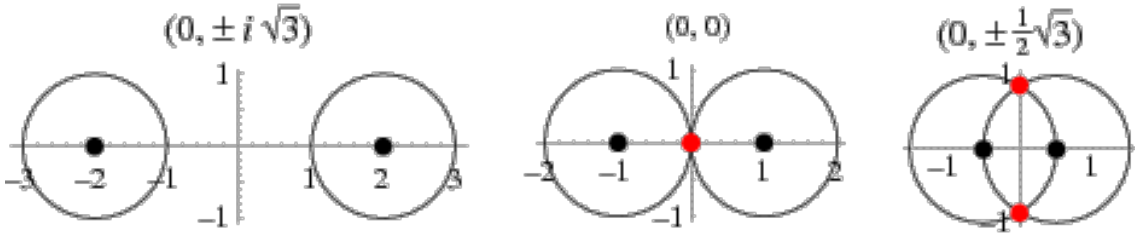


Figure 3.2.: Possible outcomes of z , given arrangement of the (non)intersecting circles. Image taken from [15]

To accommodate for this, one can calculate the shortest distance between the curves and estimate the position to be on the middle of the distance between them. This point will be on the line between the radar positions. By adding half of the gap between the radars to one of the distance vectors, one can estimate a position. This gives us the equation

$$\mathbf{x} = \mathbf{x}_{r_1} + \left(\frac{2r_1 + (d - r_2)}{2d} \right) (\mathbf{x}_{r_2} - \mathbf{x}_{r_1}) \quad (3.8)$$

The problem using the basic Trilateration approach is that the measurements produced from the radars might not be exact. Neither are the reflections coming from the center, but rather from the outer boundary of the object. Depending on the arrangement of the radars, the point estimated can be far from the 'real' point. The 'real' point here being the volume center of the person. In Fig. 3.3 we can see how this place change in accordance to the placement of the object in front of two radars and the size of the object itself.

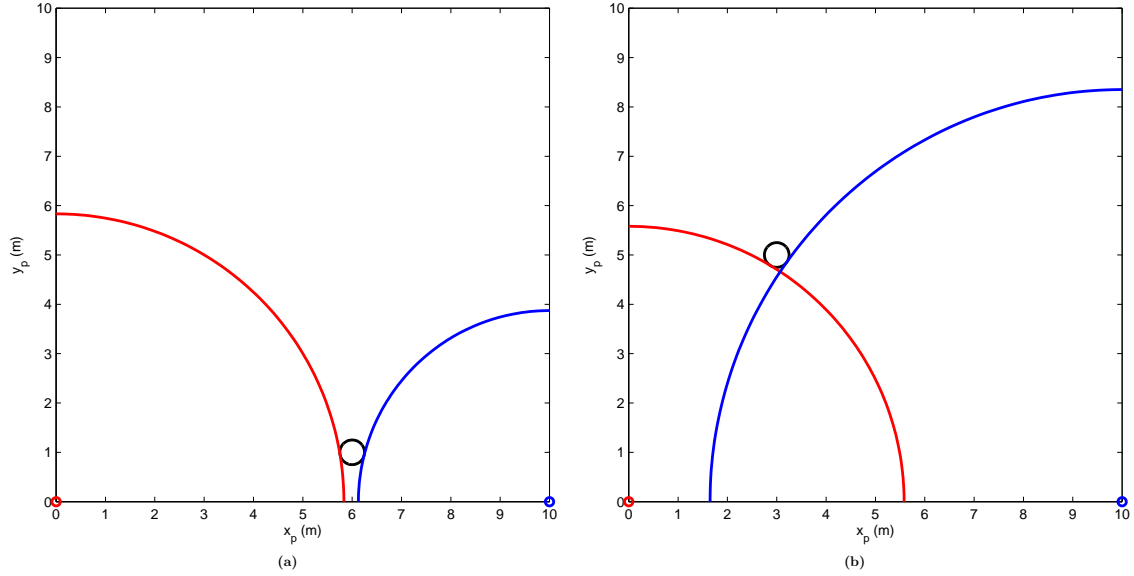


Figure 3.3.: Depending on the location and size of an object, the estimated position from Trilateration can deviate from the real position by a large amount. In both cases the radars are placed in (0,0) and (10,0), and a ball with radius 0.25m are placed at **a)** (6,1) **b)** (5,3)

3.2. Nonlinear Least Square Method

By considering the radars as satellites, we can use the same principles as in the Global Positioning Systems (GPS). By using the radar range estimates, we can utilize the Linearized Recursive Least Square method for single point position estimation, as described by Vik in [16]. Given n radars the range measurement equation is

$$r_i = \sqrt{(\mathbf{x}_{r_i} - \mathbf{x})^T (\mathbf{x}_{r_i} - \mathbf{x})} - \beta_i \quad (3.9)$$

where $i \in [1, \dots, n]$ and $\mathbf{x}_{r_i} \in \mathbb{R}^3$ is the position of the radar i , and the bias β_i , i.e the 'body distance', the distance from the outer region of the body to the volume center as seen from each radar. The volume center are described by the position vector \mathbf{x} , the position vector of the volume center of the person observed. A difference in this approach from GPS is that a GPS utilizes a clock. The clock can be slightly off and this would result in a wrong range estimate for the GPS. With the radars, there are no clock needed to synchronize the signals. The radars can only measure the boundary of an object. To accommodate for this, the β variable replaces the clock error.

To solve for \mathbf{x} , the nonlinear equation

$$\mathbf{r} = \mathbf{h}(\mathbf{x}, \beta), \quad (3.10)$$

where we have that $\mathbf{r} = [r_1, \dots, r_n]^T \in \mathbb{R}^n$ and

$$\mathbf{h}(\mathbf{x}, \tau) = \begin{bmatrix} \sqrt{(\mathbf{x}_{\mathbf{r}_1} - \mathbf{x})^T (\mathbf{x}_{\mathbf{r}_1} - \mathbf{x})} - \beta_1 \\ \vdots \\ \sqrt{(\mathbf{x}_{\mathbf{r}_n} - \mathbf{x})^T (\mathbf{x}_{\mathbf{r}_n} - \mathbf{x})} - \beta_n \end{bmatrix} \quad (3.11)$$

must be solved.

By linearize (3.9) we get

$$\Delta \rho_i = -\mathbf{l}_i^T \Delta \mathbf{x} - \beta_i \quad (3.12)$$

where

$$\mathbf{l}_i = \frac{\partial \mathbf{h}_i(\mathbf{x})}{\partial \mathbf{x}} = \frac{\mathbf{x}_{\mathbf{r}_i} - \hat{\mathbf{x}}}{\sqrt{(\mathbf{x}_{\mathbf{r}_i} - \hat{\mathbf{x}})^T (\mathbf{x}_{\mathbf{r}_i} - \hat{\mathbf{x}})}} \quad (3.13)$$

$$\mathbf{L} = \begin{bmatrix} -l_1^{x_e} & -l_1^{y_e} & -l_1^{z_e} \\ -l_2^{x_e} & -l_2^{y_e} & -l_2^{z_e} \\ \vdots & \vdots & \vdots \\ -l_n^{x_e} & -l_n^{y_e} & -l_n^{z_e} \end{bmatrix} \in \mathbb{R}^{n \times 4} \quad (3.14)$$

where \mathbf{L} is the Line of Sight matrix and $\hat{\mathbf{x}}$ is the best estimate we currently have of \mathbf{x} . $\Delta \mathbf{x}$ and $\Delta \rho$ are the position and range errors respectively. By expanding \mathbf{x} to also incorporate the body bias β , we get $\mathbf{x}_* = [\mathbf{x}^T, \beta]^T$. We can now write

$$\Delta \rho = \mathbf{L}_* \Delta \hat{\mathbf{x}}_*, \quad (3.15)$$

where

$$\mathbf{L}_* = \begin{bmatrix} -l_1^{x_e} & -l_1^{y_e} & -l_1^{z_e} & 1 \\ -l_2^{x_e} & -l_2^{y_e} & -l_2^{z_e} & 1 \\ \vdots & \vdots & \vdots & \vdots \\ -l_n^{x_e} & -l_n^{y_e} & -l_n^{z_e} & 1 \end{bmatrix} \in \mathbb{R}^{n \times 4}. \quad (3.16)$$

$\Delta \hat{\mathbf{x}}$ can now be found from

$$\Delta \hat{\mathbf{x}} = \mathbf{L}_*^\dagger \Delta \rho \quad (3.17)$$

where $\mathbf{L}_*^\dagger = [\mathbf{L}_*^T \mathbf{L}_*]^{-1} \mathbf{L}_*^T$, is the pseudo-inverse. By utilizing the recursive least square method we get the next estimate

$$\hat{\mathbf{x}}_{n+1} = \hat{\mathbf{x}}_n + \Delta \hat{\mathbf{x}}. \quad (3.18)$$

We run the iterations for a fixed number of times in order to make the run time of the system predictable.

Murphy and Hereman [10], use a different approach to the pseudo-inverse by utilizing the singular value decomposition method (SVD). The SVD based pseudo-inverse of \mathbf{L} can be written as $\mathbf{L}^+ = \mathbf{V}\mathbf{S}^+\mathbf{U}^T$. The matrices \mathbf{U} and \mathbf{V} are unitary matrices generated by the SVD of \mathbf{L} . \mathbf{L} can be written on the form

$$\mathbf{L} = \mathbf{U}\mathbf{S}\mathbf{V}^T \quad (3.19)$$

$$\mathbf{L}^+ = \mathbf{V}\mathbf{S}^+\mathbf{U}^T \quad (3.20)$$

where $\mathbf{L}, \mathbf{\Sigma} \in \mathbb{R}^{m \times n}$, $\mathbf{U} \in \mathbb{R}^{m \times m}$ and $\mathbf{V} \in \mathbb{R}^{n \times n}$. \mathbf{S} consists of the non-zero eigenvalues of \mathbf{L} on its diagonal in descending order. The matrix \mathbf{S}^+ becomes $\mathbf{S}^+ \in \mathbb{R}^{n \times m}$, and its diagonal entries are the inverse of the eigenvalues. i.e

$$\mathbf{S} = \begin{bmatrix} 2 & 0 \\ 0 & 1 \\ 0 & 0 \end{bmatrix}, \mathbf{S}^+ = \begin{bmatrix} 0.5 & 0 & 0 \\ 0 & 1 & 0 \end{bmatrix}. \quad (3.21)$$

Murphy and Hereman [10] state that the use of the SVD pseudo-inverse does not fare better compared to the original pseudo inverse when the results are close to the real \mathbf{x} . But, it is less likely to become singular. Still, the matrix comes close, and the resulting estimates are too large to be considered acceptable.

An important difference from satellites to the use of close range radars, is that in the case of satellites the distances are approximately 20 000 km and \mathbf{L} is very little sensitive to position errors. It can therefore be considered constant, since \mathbf{l}_i is the line of sight vector and there are relative little change when a target is moving. In the case of the close range radar, the area of operation is within an area of usually less than (10m)³. Therefore, the \mathbf{L} matrix varies depending on the position of the observed person.

The RLS method applied to short distances is also dependent on a good initial estimate. As for GPS, one can have the initial estimate off by several thousand meters. At the short range, if the estimates are off by only a couple of meters, the algorithm will not converge to a solution.

3.2.1. Finding a good initial estimate

In their 1994 paper, Y.T Chan and K.C Ho [17] proposes a simple, yet efficient estimator for hyperbolic localization. The estimator utilizes a Maximum Likelihood (ML) method to give a Weighted Least Square (WLS) estimate. It is also based on the Time Difference of Arrival (TDOA) of a signal from a source between several receivers. The available measurements are $r_i - r_j$, where i and j are different receivers. In his project thesis, Jørgensen [8] adjusted the estimator to the case of

Time of Arrival (TOA) in 2D. This is better suited for our use, as the radars can calculate the time between a signal is sent and the return reflection arrives. Thus, the radar can itself calculate the TOA i.e radar i can calculate r_i . As we are interested in the height, the method is expanded to 3D by adding the z variable.

By assuming N radars, we have that equation (3.1) becomes

$$(x - x_i)^2 + (y - y_i)^2 + (z - z_i)^2 = r_i^2, \quad i = 1, 2 \dots N. \quad (3.22)$$

Fully expanded the equation becomes

$$x^2 + y^2 + z^2 - 2 \cdot x \cdot x_i - 2 \cdot y \cdot y_i - 2 \cdot z \cdot z_i = r_i^2 - x_i^2 - y_i^2 - z_i^2. \quad (3.23)$$

We are now able to create a set of linear equation for x , y and z by subtracting range measurement i from range measurement j . By doing so, we eliminate the square parts of the position estimates x^2 , y^2 and z^2 . The linear equation becomes

$$x_{i,j} \cdot x + y_{i,j} \cdot y + z_{i,j} \cdot z = \frac{1}{2} (K_j - K_i), \quad (3.24)$$

where $K_i = r_i^2 - x_i^2 - y_i^2 - z_i^2$ and the variables $x_{ij} = x_i - x_j$ with the same notation for y_{ij} and z_{ij} . What we are now left with is a set of $\frac{N!}{2(N-2)!}$ combinations of equation (3.24). With this subtraction we now have only $N-1$ linearly independent equations, seeing as using an equation not in the $\{N-1\}$ equation set, the same equation can be constructed from a linear combination from $\{N-1\}$. Thus, by doing the subtraction, we have lost one degree of freedom to solve the unknown variables.

To create the $\{N-1\}$ equation set we choose to subtract the first equation from the remaining equations.

$$x_{1,j} \cdot x + y_{1,j} \cdot y + z_{1,j} \cdot z = \frac{1}{2} (K_j - K_1). \quad (3.25)$$

We now construct the WLS estimate of the true positions. We define the matrices

$$\mathbf{b} = \begin{bmatrix} \frac{1}{2} (K_2 - K_1) \\ \frac{1}{2} (K_3 - K_1) \\ \vdots \\ \frac{1}{2} (K_N - K_1) \end{bmatrix}$$

$$\mathbf{M} = \begin{bmatrix} x_{12} & y_{12} & z_{12} \\ x_{13} & y_{13} & z_{13} \\ \vdots & \vdots & \vdots \\ x_{1N} & y_{1N} & z_{1N} \end{bmatrix}$$

$$\mathbf{x} = \begin{bmatrix} x \\ y \\ z \end{bmatrix}$$

Thus, the error can be defined as

$$\psi = \mathbf{b} - \mathbf{M}\mathbf{x} \quad (3.26)$$

and

$$\mathbf{\Psi} = \mathbf{E}[\psi\psi^T]$$

The WLS then becomes

$$\hat{\mathbf{x}} = (\mathbf{M}\mathbf{\Psi}^{-1}\mathbf{M}^T)^{-1}\mathbf{M}^T\mathbf{\Psi}^{-1}\mathbf{b} \quad (3.27)$$

As Jørgensen [8] mentions, any additional combination of the $\frac{N!}{2(N-2)!}$ equations in \mathbf{h} will produce the same $\mathbf{\Psi}$. This is because the equations are not linearly independent. Given the correct placement of radars and that the number of unknown position coordinates, $\mathbf{x} \in \mathbb{R}^n$, as long as the number of radars used are $n+1$, then the matrix \mathbf{M} are square and invertible. Therefore, by using the properties of inverted square matrices we have that $(\mathbf{A}_1\mathbf{A}_2 \dots \mathbf{A}_k)^{-1} = \mathbf{A}_k^{-1} \dots \mathbf{A}_2^{-1}\mathbf{A}_1^{-1}$. By utilizing this property, we can greatly reduce the complexity of equation (3.27) to

$$\hat{\mathbf{x}} = (\mathbf{M}\mathbf{\Psi}^{-1}\mathbf{M}^T)^{-1}\mathbf{M}^T\mathbf{\Psi}^{-1}\mathbf{b} = \mathbf{M}^{-1}\mathbf{\Psi}(\mathbf{M}^T)^{-1}\mathbf{M}^T\mathbf{\Psi}^{-1}\mathbf{b} = \mathbf{M}^{-1}\mathbf{b} \quad (3.28)$$

Thus resulting in the Linear Least Square estimate of position, and we have an initial estimate to use for the Nonlinear Least Square method.

When we only have 3 radars we only get an estimate for x and y . The remaining z are set to zero.

3.3. Human Movement Model

A human being is a complex system with a lot of moving parts. Therefore, a common simplification is to describe the moving human as a point, with position coordinates, velocity and acceleration. This point would be somewhere inside the body of the person observed. In Jørgensen's project thesis [8], he proposes a human movement model for a two dimensional movement in x and y . This model is used and expanded to incorporate the height position, z . The human state vector, \mathbf{x} , is also expanded with the acceleration a in each direction

$$\mathbf{x} = \begin{bmatrix} x & y & z & v_x & v_y & v_z & a_x & a_y & a_z \end{bmatrix}^T. \quad (3.29)$$

A natural model taking in account changes in velocity is the continuous random walk model given by

$$\dot{\mathbf{x}} = \begin{bmatrix} \dot{x} \\ \dot{y} \\ \dot{z} \\ \dot{v}_x \\ \dot{v}_y \\ \dot{v}_z \\ \dot{a}_x \\ \dot{a}_y \\ \dot{a}_z \end{bmatrix} = \begin{bmatrix} v_x \\ v_y \\ v_z \\ a_x \\ a_y \\ a_z \\ w_1 \\ w_2 \\ w_3 \end{bmatrix} = \begin{bmatrix} 0 & 0 & 0 & 1 & 0 & 0 & 0 & 0 & 0 \\ 0 & 0 & 0 & 0 & 1 & 0 & 0 & 0 & 0 \\ 0 & 0 & 0 & 0 & 0 & 1 & 0 & 0 & 0 \\ 0 & 0 & 0 & 0 & 0 & 0 & 1 & 0 & 0 \\ 0 & 0 & 0 & 0 & 0 & 0 & 0 & 1 & 0 \\ 0 & 0 & 0 & 0 & 0 & 0 & 0 & 0 & 1 \\ 0 & 0 & 0 & 0 & 0 & 0 & 0 & 0 & 0 \\ 0 & 0 & 0 & 0 & 0 & 0 & 0 & 0 & 0 \\ 0 & 0 & 0 & 0 & 0 & 0 & 0 & 0 & 0 \end{bmatrix} \mathbf{x} + \begin{bmatrix} 0 & 0 & 0 \\ 0 & 0 & 0 \\ 0 & 0 & 0 \\ 0 & 0 & 0 \\ 0 & 0 & 0 \\ 0 & 0 & 0 \\ 1 & 0 & 0 \\ 0 & 1 & 0 \\ 0 & 0 & 1 \end{bmatrix} \mathbf{w}. \quad (3.30)$$

$\dot{\mathbf{x}}$ is the time derivative of \mathbf{x} , and the process disturbance vector $\mathbf{w} = [w_1, w_2, w_3]^T$ is linearly independent zero mean Gaussian white noise to describe the 'jerk' in acceleration that occurs in each direction. The variance is set to be equal in the all directions i.e $\sigma_{w_1}^2 = \sigma_{w_2}^2 = \sigma_{w_3}^2$. As this point-modeling describes the movement of the person or 'point' in a coordinate frame that is sett in the room, it does not take into account rotation, or turning, and as such the variance in x and y direction is equal. By applying the first order Taylor approximation we get the discrete model from continuous case

$$\mathbf{x}(k+1) = \begin{bmatrix} 1 & 0 & 0 & h & 0 & 0 & \frac{h^2}{2} & 0 & 0 \\ 0 & 1 & 0 & 0 & h & 0 & 0 & \frac{h^2}{2} & 0 \\ 0 & 0 & 1 & 0 & 0 & h & 0 & 0 & \frac{h^2}{2} \\ 0 & 0 & 0 & 1 & 0 & 0 & h & 0 & 0 \\ 0 & 0 & 0 & 0 & 1 & 0 & 0 & h & 0 \\ 0 & 0 & 0 & 0 & 0 & 1 & 0 & 0 & h \\ 0 & 0 & 0 & 0 & 0 & 0 & 1 & 0 & 0 \\ 0 & 0 & 0 & 0 & 0 & 0 & 0 & 1 & 0 \\ 0 & 0 & 0 & 0 & 0 & 0 & 0 & 0 & 1 \end{bmatrix} \mathbf{x}(k) + \begin{bmatrix} \frac{h^3}{6} & 0 & 0 \\ 0 & \frac{h^3}{6} & 0 \\ 0 & 0 & \frac{h^3}{6} \\ \frac{h^2}{2} & 0 & 0 \\ 0 & \frac{h^2}{2} & 0 \\ 0 & 0 & \frac{h^2}{2} \\ h & 0 & 0 \\ 0 & h & 0 \\ 0 & 0 & h \end{bmatrix} \mathbf{w}(k) \quad (3.31)$$

with h as the process time step. It is important to tune the time step in advance when using the model. Tuning must be done by noting the rate of observations available for each second when running the system. This model will be the basis for the state estimating Kalman Filter that will be explained in the next section.

3.4. The Kalman Filter

As the only states we can measure are the position states, we need to estimate the remaining states. For this purpose we utilizes he Kalman Filter. The Kalman Filter

is a widely used filter for optimal state estimation and is a natural basis for any state estimation. There are a lot of literature available on the subject of Kalman Filtering, but this section is based of the books by Fossen [18] and Brown [19].

The principle behind the Kalman Filter is that it predicts the state and covariance given an underlying model and prior states estimates. By using observations, it can correct and update the predicted estimates and covariance. The system is on the form of

$$\mathbf{x}_{k+1} = \mathbf{F}_k \mathbf{x}_k + \mathbf{E}_k \mathbf{w}_k, \quad (3.32)$$

$$\mathbf{y}_k = \mathbf{H}_k \mathbf{x}_k + \mathbf{v}_k \quad (3.33)$$

where \mathbf{F}_k and \mathbf{E}_k are the matrices in (3.31), and \mathbf{w}_k and \mathbf{v}_k are the Gaussian distributed white noise vectors with covariance design matrices \mathbf{Q}_k and \mathbf{R}_k respectively. We set $\mathbf{Q}_k = \sigma_w^2 \mathbf{I}_{3 \times 3}$, and \mathbf{R}_k to be $\sigma_v^2 \mathbf{I}_{3 \times 3}$, where $\sigma_v^2 = 0.1$. Since the only observed states are the x,y and z position estimated from the Nonlinear Least Square algorithm, the observation matrix \mathbf{H}_k is

$$\mathbf{H}_k = \begin{bmatrix} 1 & 0 & 0 & 0 & 0 & 0 & 0 & 0 & 0 \\ 0 & 1 & 0 & 0 & 0 & 0 & 0 & 0 & 0 \\ 0 & 0 & 1 & 0 & 0 & 0 & 0 & 0 & 0 \end{bmatrix}. \quad (3.34)$$

The a priori prediction is on the form of

$$\hat{\mathbf{x}}_{k|k-1} = \mathbf{F}_k \hat{\mathbf{x}}_{k-1|k-1} \quad (3.35)$$

$$\hat{\mathbf{P}}_{k|k-1} = \mathbf{F}_k \hat{\mathbf{P}}_{k-1|k-1} \mathbf{F}_k^T + \mathbf{E}_k \mathbf{Q}_k \mathbf{E}_k^T \quad (3.36)$$

And the a posteriori estimate updates are on the form

$$\mathbf{K}_k = \hat{\mathbf{P}}_{k|k-1} \mathbf{H}_k^T \left[\mathbf{H}_k \hat{\mathbf{P}}_{k|k-1} \mathbf{H}_k^T + \mathbf{R}_k \right]^{-1} \quad (3.37)$$

$$\hat{\mathbf{x}}_{k|k} = \hat{\mathbf{x}}_{k|k-1} + \mathbf{K}_k \left[\mathbf{y}_k - \mathbf{H}_k \hat{\mathbf{x}}_{k|k-1} \right] \quad (3.38)$$

$$\hat{\mathbf{P}}_{k|k} = [\mathbf{I} - \mathbf{K}_k \mathbf{H}_k] \hat{\mathbf{P}}_{k|k-1} [\mathbf{I} - \mathbf{K}_k \mathbf{H}_k]^T + \mathbf{K}_k \mathbf{R}_k \mathbf{K}_k^T \quad (3.39)$$

The output state vector $\hat{\mathbf{x}}_{k|k}$ is the estimates used to decide whether or not a fall have occurred. This will be described in chapter 6.

3.5. Radar Placements

In their paper, [20], S.Zhao et.al. analytically characterizes optimal sensor placement for target localization and tracking in both 2D and 3D. The paper concludes that for 2D tracking of a specific point with sensors influenced by noise, a sensor placement in an equilateral arrangement with the point of observation in the middle of the triangle. When the target are located in 3D, the optimal placement are in an equilateral prism arrangement. Both are shown in Fig. 3.4.

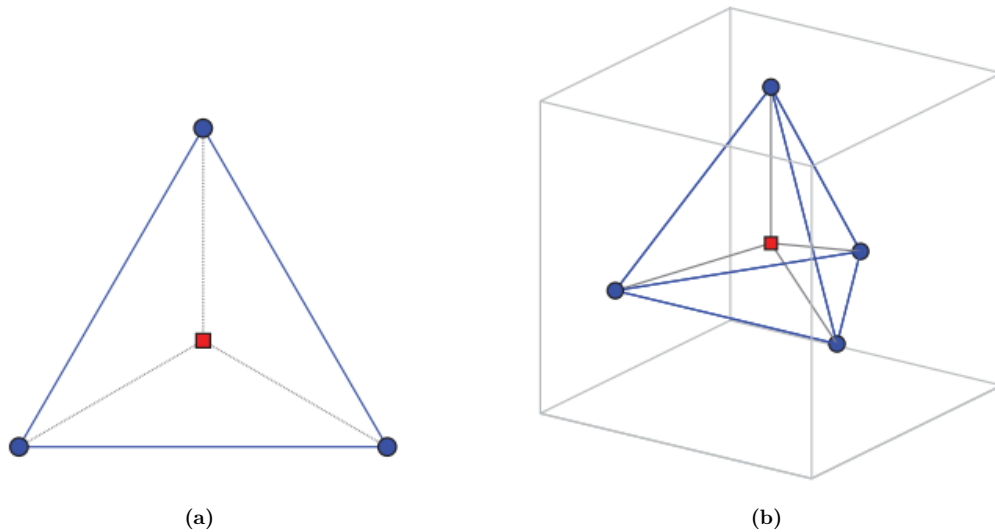


Figure 3.4.: Optimal sensor placement for a given target localization. **a)** Three sensors for a 2D location. **b)** Four sensors for a 3D location

Given the directionality of the Vivaldi antennas used, the placement of the fourth radar would be in the bottom corner. This is chosen to get a larger coverage area where all the antennas coincide.

4. Testing

This section present the the setup and performance of the real physical testing of the system. Only raw data were acquired during these tests, and the methods for localization and tracking were applied later. As only three radars were available at the time of the thesis, the result can only give an idea of how the system will work. There are also an absence of verification equipment. Thus, there are no form of comparison of the estimates generated to known values. All equipment used are listed in Appendix B.

4.1. Setup

Room G238 in “Gamle Electro” were utilized to enact different fall scenarios in front of radars. A mattress were placed on the floor in the middle of the room. The radars were then spaced out, and the origin of the coordinate frame were chosen to be on the floor below one of the radars. The distances between them and height above ground were measured using a tape measure. The radar placement given in coordinates with radar 3 as reference, but with the floor as 0 for z . are shown in Tab. 4.1

	x	y	z
Radar 1	0.2 m	3.4 m	1.43 m
Radar 3	2.2 m	3.4 m	1.43 m
Radar 3	0 m	0 m	0.7 m

Table 4.1.: Radar Position as placed in the room with the origin of the coordinate system chosen to be located below Radar 3.

A challenge with testing, is that the radars do not come with tools or casing to properly place them in an environment. The Vivaldi antennas are planar and have a directional spread. They are directly coupled to the radar with SMA connectors, which is rather fragile. Because of this, it were difficult to attain a good orientation of the radars. Nonetheless, the radars were placed on top of two tables stacked on top of each other and directed towards a common area as shown in Fig. 4.1.

There are no other form of communications between the radars and the PC besides USB. Therefore, because of the distances between the radars, additional USB cables

were needed beside the ones that already comes with the radar module. The cables that were utilized were 5m long USB cables with signal amplifiers to avoid signal loss. The additional length made it more easy to secure the radars in a fixed position and avoid movement of the antennas, by simply tie the USB cable to the table legs.

On a side note; Novelda have a new radar module under development and is planning to add a Wi-Fi module to the radar, as well as batteries. This may make future experiments more easily conducted.

4.2. Test Scenarios

Walking with fall forward

In this scenario, the test person are walking in y direction with a relatively constant velocity. At one point the person stumbles and falls straight forward in what can be described as a vertical pole tipping over. The person are avoiding to catch the fall.

It can be seen in Fig. 4.2, as long as the person is within the area covered by all the radars the tracking algorithms give results that mimics the real movement of the person. However, it only presents a two dimensional position and are zero in the height estimation. Thus, we can not see any change in the height estimate beside a small change at a period of the testing where the fall did not occur. The change that can be seen in Fig. 4.2 **b)** are from when the Kalman Filter becomes initialized. This happens when all of the three radars have detected movement and have estimated a range.

Walking with fall to the side

In this scenario, the test person are walking in y direction with a relatively constant velocity. At one point the person stumbles and falls to the side in x direction. It can also be described as a vertical pole tipping over. The person are avoiding to catch the fall.

It can be seen from Fig. 4.3 the result are similar to the previous test. The tracking work in the xy -plane, but no values other than zero in the z -plane.

Walking with leg giving in

In this scenario, the test person are walking in y direction with a relatively constant velocity. At one point the person's left leg gives way and falls to the side in x direction with a small amount of rotation and ends on his back. The person are avoiding to catch the fall.

Some times during the test the position estimates put the person outside of the room used.

Discussing the results

As the results from sec. 4.2 show, the placement of the radars did not result in a possible height estimation. The directionality of the Vivaldi antennas also effected the test, as the test person would walk outside of the are covered by all of the radars. This resulted in range estimates being stationary and sometimes the localization estimates were outside of the room.

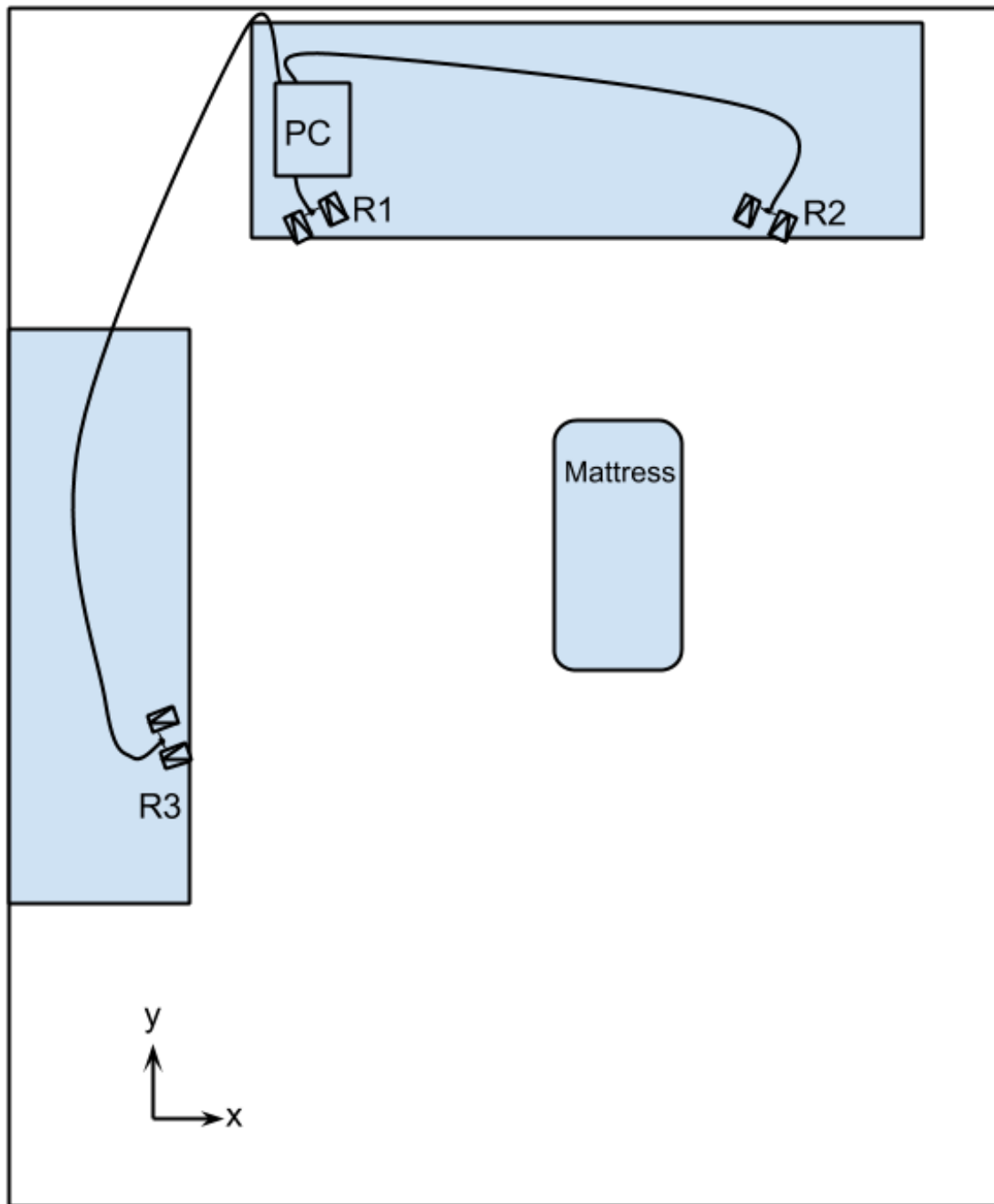


Figure 4.1.: Test Setup: The radars annotated with the R1,R2 and R3. The origin of the coordinate system is located below R3. R1 and R2 are placed at a higher level than R3. The mattress on the floor were used to soften the impact of the fall. The PC were located outside the area the radars cover.

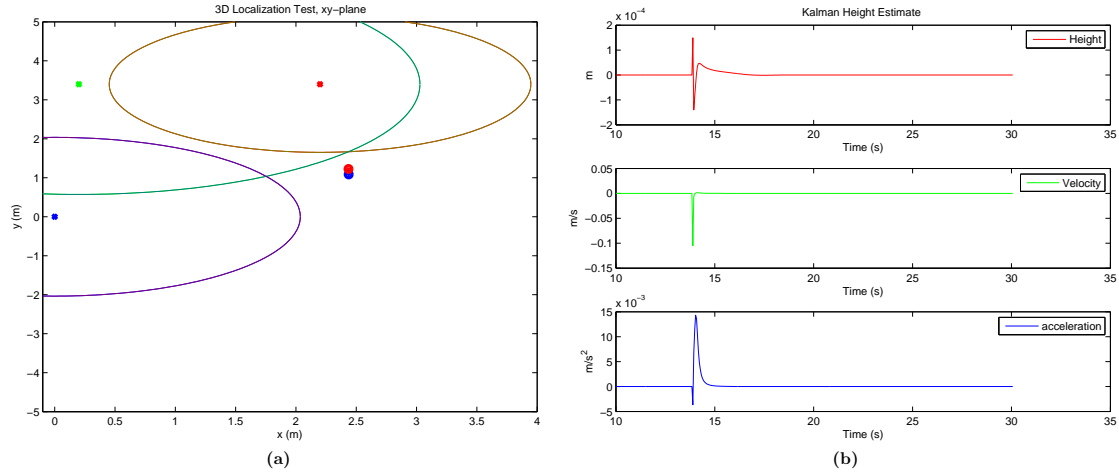


Figure 4.2.: Test 1: Walking with fall forward . **a)** Location estimate from Weighted Least Square. The radar positions are indicated by the points in the center of the circles. The circles are the estimated range for each radar. The red dot outside the circles are the estimate generated by the Least Square method, and the blue dot are the Kalman filtration of this point. **b)** The Kalman estimated states of z throughout the test. It can be seen that the estimates are centered around zero.

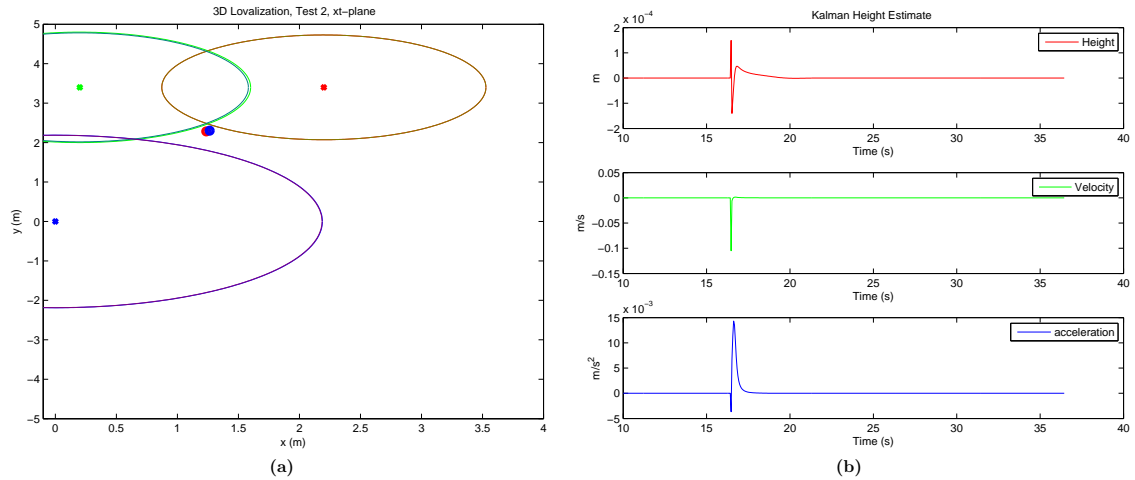


Figure 4.3.: Test 3: Walking with left leg giving in . **a)** Location estimate from Weighted Least Square. The radar positions are indicated by the points in the center of the circles. The circles are the estimated range for each radar. The red dot outside the circles are the estimate generated by the Least Square method, and the blue dot are the Kalman filtration of this point. **b)** The Kalman estimated states of z throughout the test. It can be seen that the estimates are centered around zero.

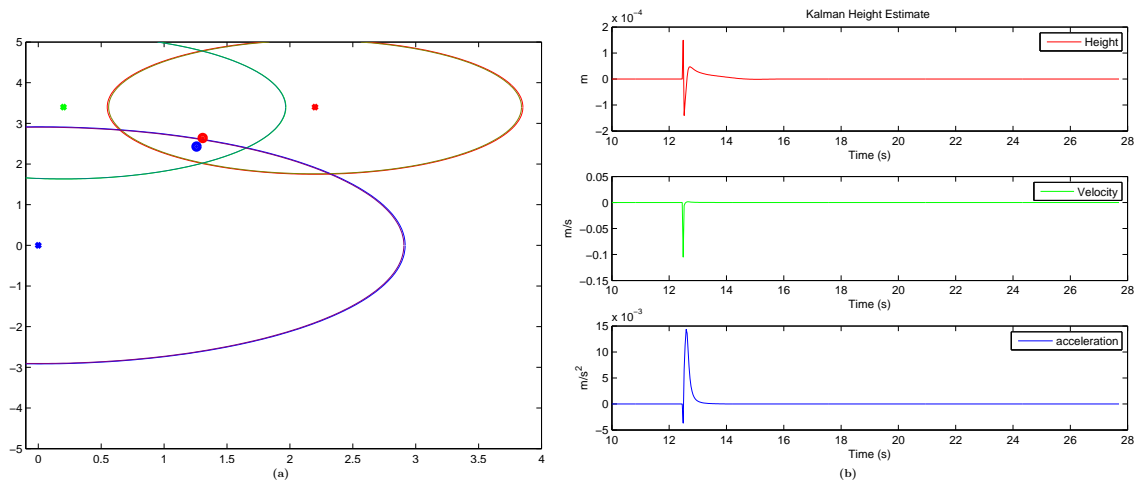


Figure 4.4.: Test 3: Walking with fall to the side . **a)** Location estimate from Weighted Least Square. The radar positions are indicated by the points in the center of the circles. The circles are the estimated range for each radar. The red dot outside the circles are the estimate generated by the Least Square method, and the blue dot are the Kalman filtration of this point. **b)** The Kalman estimated states of z throughout the test. It can be seen that the estimates are centered around zero.

5. Simulation

Because of the physical limitations in the testing, it was difficult to gather the data from the desired radar setup. We will therefore do numerical simulations to verify that the methods and radar setup will work under more ideal conditions. In all simulations, it is assumed that the radars are perfectly monostatic and uses omnidirectional antennas. Monostatic means that the sending and receiving of a signal occurs at the same point. Omnidirectional means that the signal spreads out as a perfect sphere from the point of the radar. We examine the accuracy of the estimation of the position vector \mathbf{x} . We run simulations using three radars for different scenarios of object behavior. These scenarios are; Horizontal movement below the radar plane. Horizontal movement in the radar plane. And oscillating vertically movement in or below the plane. We run these simulations with and without noise.

Lastly, we will expand from a point to a sphere. The radars measures to the boundary of the body. By subtracting a constant value from the range estimate made in the zero noise scenario, we get the sphere. A sphere is a lot less complex structure to measure compared to a human body, but is a good approximation to a human head. Thus, it might not be an exact model of the a full body, but shows the principles behind the methods. More complex methods are necessary to be able to discern between limbs and a torso. Limbs, such as feet and hands, might give a shorter range estimate to one of the radars that observes it. This would effect position estimate. We also test this scenario using four radars. The simulations uses the Weighted Least Square method for initial estimate to the Nonlinear Least Square.

5.1. Point Object Simulation

In this section we assume that there exist a point in the room that the radars get a reflection from. The reflections are then assumed received, and that the range estimation method of pulse spectrum signature matching gives the correct distance for each radar for the zero noise simulations. In the noise simulations, it is assumed that the range estimates contains uniformly distributed noise that varies between ± 0.05 . These ranges are used with the equations for a Least Square estimate from equation (3.28). The resulting estimate $\hat{\mathbf{x}}$, are then used as the initial estimate for the Nonlinear Least Square method of position estimation, and is iterated upon for 10 iterations to produce the final estimate of \mathbf{x} . This section uses three radars to

determine the position of a point. We place the radars in three of the four corners of the ceiling. The position coordinates of the radars are given according to Tab. 5.1. The origin of the reference frame is chosen to be on the floor below Radar 1. It is also assumed that the floor is $10\text{m} \times 10\text{m}$ in area, and the ceiling, $z_c = 2.5\text{m}$ high. With the given number of radars available, the Nonlinear Least Square method uses the \mathbf{L} matrix from equation.(3.14)

	Radar 1	Radar 2	Radar 3
x	0 m	10 m	0 m
y	0 m	5 m	10 m
z	2.5 m	2.5 m	2.5 m

Table 5.1.: Radar placement chosen for the simulations

5.1.1. Zero Noise

We now run the simulations without added noise.

Scenario 1: Horizontal Movement $z < z_c$

The movement of the point of observation and the resulting deviation from the true value of the height are shown here when there are 3 radars observing. The left images are the position and height of the simulated object and the right images are the resulting error in the estimates. As seen here, the errors that occurs are in the 10^{-14}m and can be considered zero. These errors are most likely due to rounding errors in the PC.

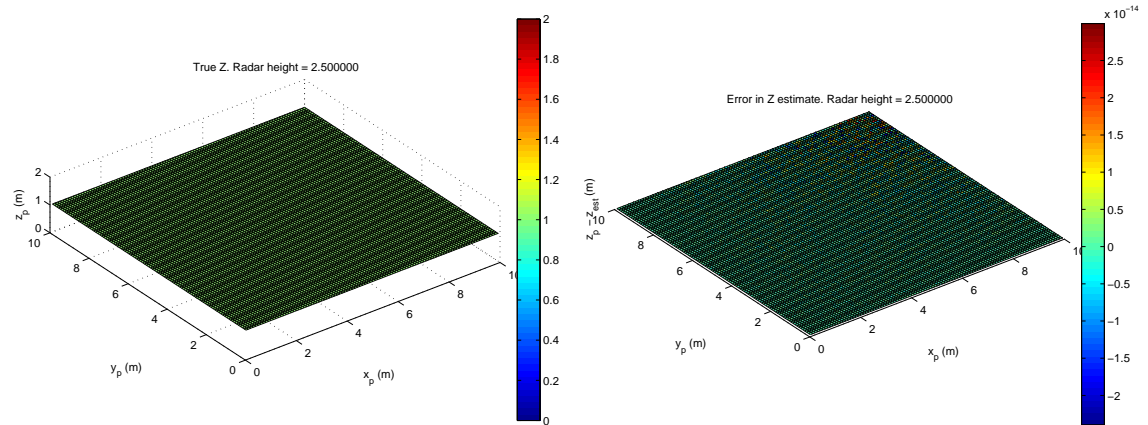


Figure 5.1.: Horizontal Movement $z < z_c$: z moves in a parallel plane below the radar plane. True z in the right image. Left image show $z - \hat{z}$.

Scenario 2: Horizontal Movement $z = z_c$

The observation point are moving in the same xy-plane as the radars span. As the previous scenario, the resulting errors are small considering the use of the measurement. However, they are already significantly larger compared to the scenario where the object moved in a plane below the radars.

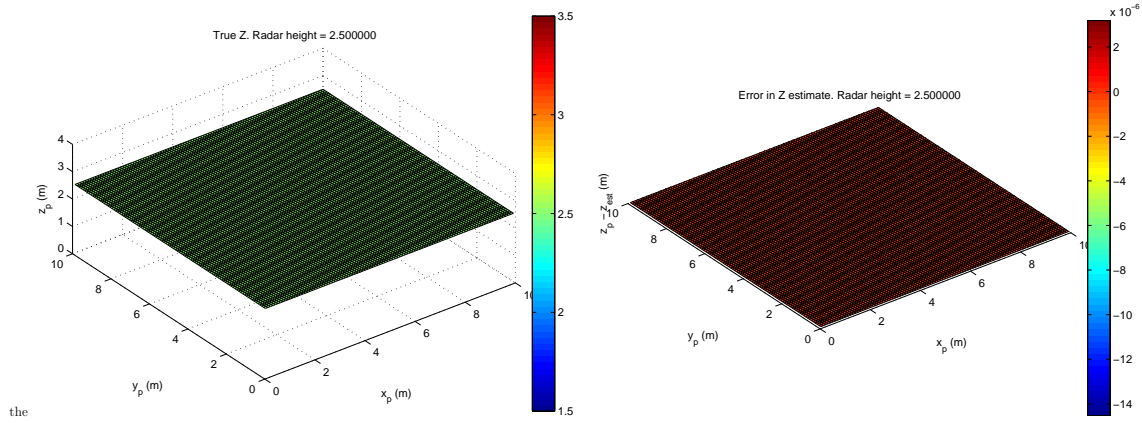


Figure 5.2.: Horizontal Movement $z = z_c$: z moves in the same plane as the radar plane. True z in the right image. Left image show $z - \hat{z}$.

Scenario 3: Oscillating Movement $z \leq z_c$

The observation point are moving up and down, reaching the xy-plane of the radars. The resulting deviations are due to rounding errors and are in the scales of 10^{-14} m and can be considered negligible when it comes to position estimating.

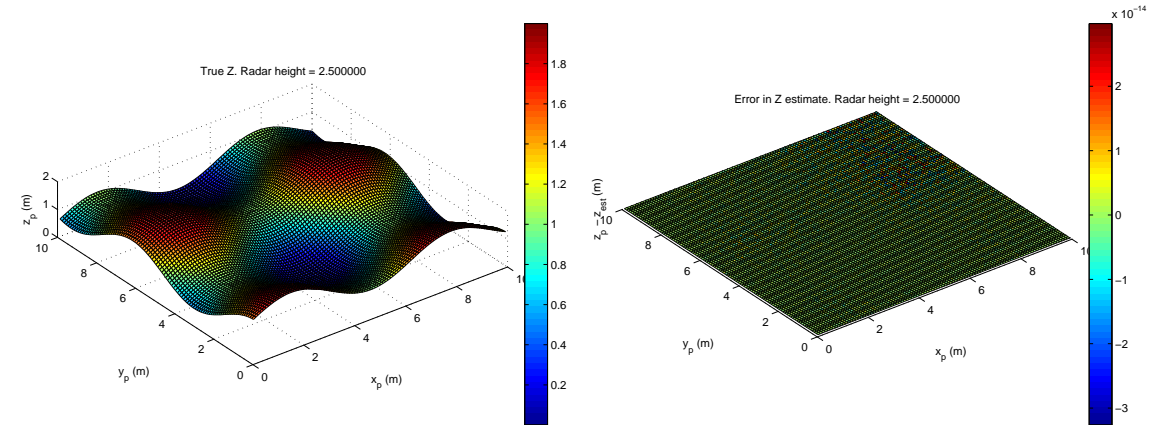


Figure 5.3.: Oscillation Movement $z \leq z_c$: z moves in a sinusoidal wave pattern in a plane below the radar plane. True z in the right image. Left image show $z - \hat{z}$.

By implementing the Weighted Least Square and the Nonlinear Least square methods and simulating, we can see that there are no problem to find the correct height and position for this arrangement of radars, or position of the observed point. As the right images show in the figures in the scenarios above. The deviations are in the sizes of 10^{-6}m to 10^{-14}m , and can be considered negligible when it comes to determine if an object have fallen or not. The deviations can be contributed to accuracy in computation

5.1.2. Noise Scenario

When we introduce an uniformly distributed noise with ranging between 0.05m to -0.05m , to the range estimate we can observe a large increase in error from the estimated height to the real height. When the point of observation is at a constant distance of about 1.5m we have errors in the ranges of about 1m .

Scenario 1: Horizontal Movement $z < z_c$

We have that the point of observation are moving only in the xy plane and the height are constant. It can be seen that the errors are quite large, ranging up towards a meter in deviation, even though the errors in range measurements are small.

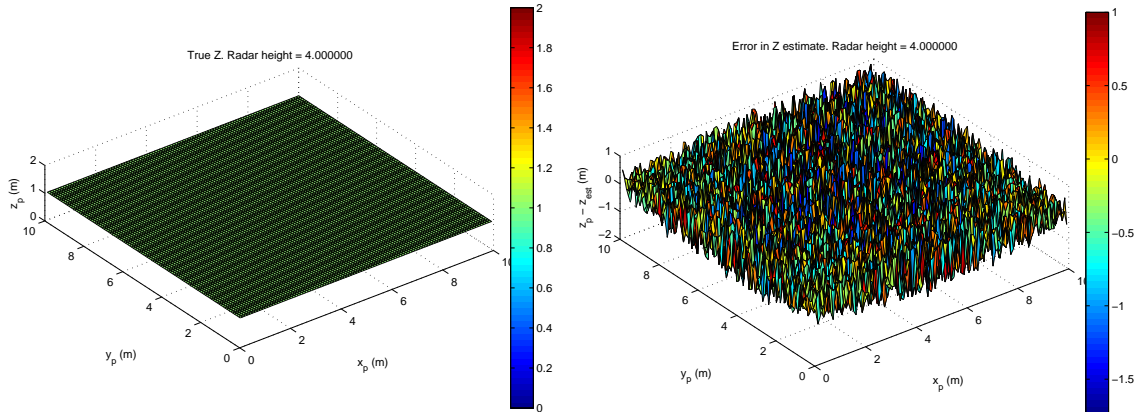


Figure 5.4.: Horizontal Movement $z < z_c$: z moves in a plane below the radar plane. Uniformly distributed noise is added to the range measurements. True z in the right image. Left image show $z - \hat{z}$.

Scenario 2: Horizontal Movement $z = z_c$

The observation point are moving in the same xy-plane as the radars span, and at several estimation points they are non existent. The algorithm outputs 'Not a Number', as line of sight matrix \mathbf{L} becomes singular and no estimates from the NLS are available.

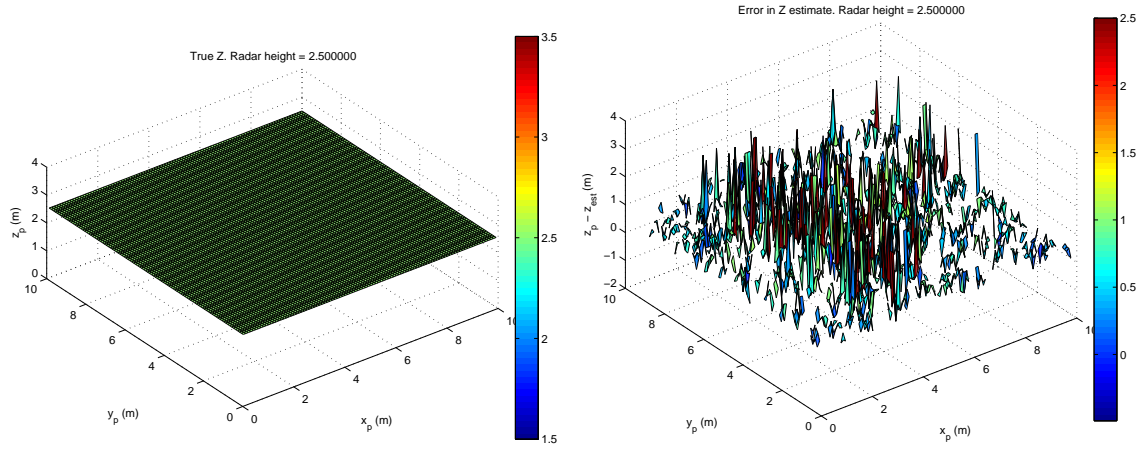


Figure 5.5.: Horizontal Movement $z = z_c$: z moves in the same plane as the radars span. Uniformly distributed noise is added to the range measurements. True z in the right image. Left image show $z - \hat{z}$.

Scenario 3: Oscillation Movement $z \leq z_c$

In Fig. 5.6 we see that the observation point are moving up and down in a steady fashion, with the max height reaching the xy-plane of the radars. As seen from the images of the noise, the \mathbf{L} matrix again becomes singular in the areas when the observation point reaches the radar plane. Otherwise, in the lower regions the errors are around zero.

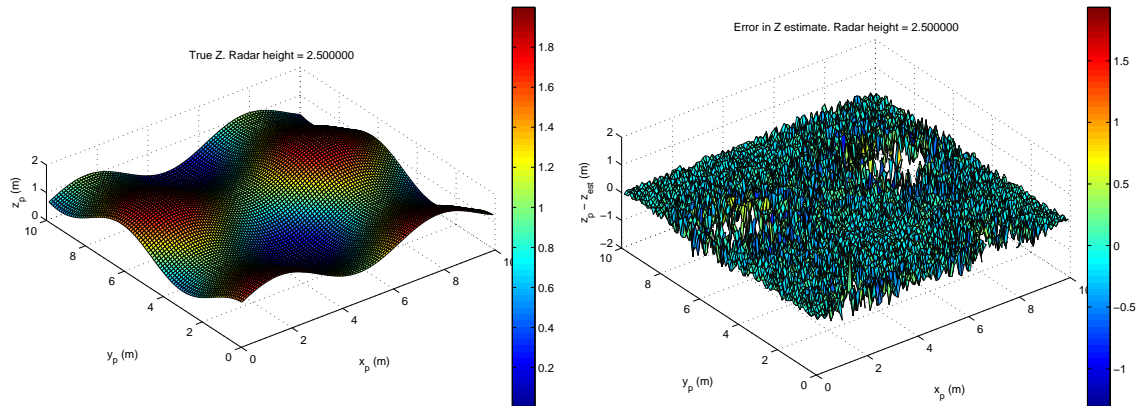


Figure 5.6.: Oscillation Movement $z \leq z_c$: z moves in a wave pattern. Uniformly distributed noise is added to the range measurements. True z in the right image. Left image show $z - \hat{z}$.

5.2. Spherical Object Simulation

In this section we expand the point into a sphere, and assume that there exist an object in the room that the radars get a reflection from. The reflections are then assumed received, and that the range estimation method of pulse spectrum signature matching gives the correct distance for each radar to the surface of the object. The object is now introducing a bias in the range estimates. In this simulation we assume that the closest body part are the range estimate. With the radar placed in the ceiling, the head is the most likely body part to be closest to the radars. Therefore, we simulate the head as a sphere with radius 0.07m. From Statistisk Sentral Byrå [21], we have that the average height of male recruits in 2007 were 179,9 cm. The number is probably higher than the average of the entire population, but is a good estimate of a normal height. Therefore, we place the center of the sphere at 1.73m, so that the top of the 'head' is at approximately the same height. The simulations are done with two different room sizes, 10m x 10m and 4m x 4m with ceiling height set to $z_c = 2.5$ m, and are done using both three and four radars. An illustration of the conditions are shown in Fig. 5.7.

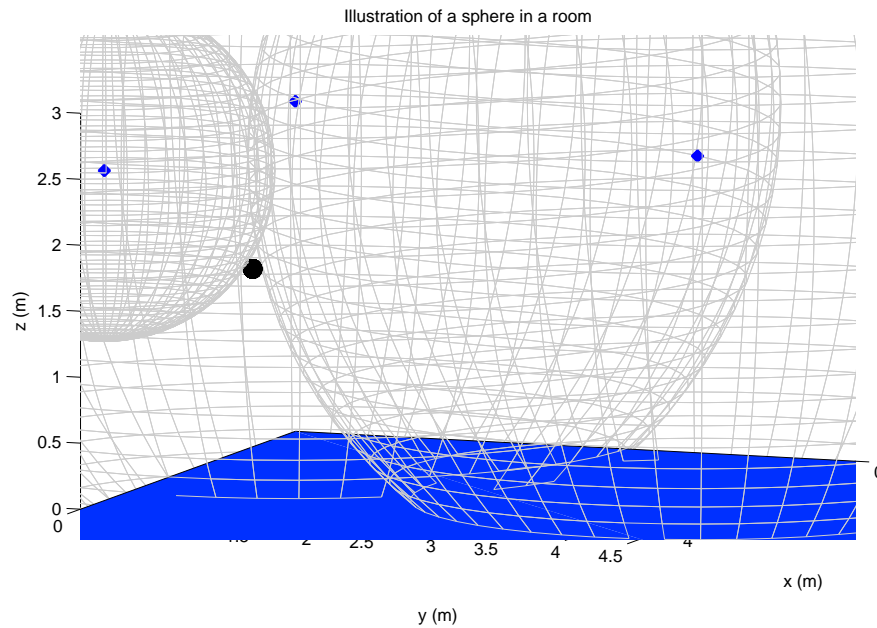


Figure 5.7.: Illustration of a sphere in a 4m x 4m room with a ceiling height of 2.5m. The black sphere have a radius of 0.07m. The blue radars are placed according to Tab. 5.1.

5.2.1. 3 Radars

10m x 10m Room

With the room chosen to be as in the previous simulations we place the radar in the same locations given in Tab. 4.1.

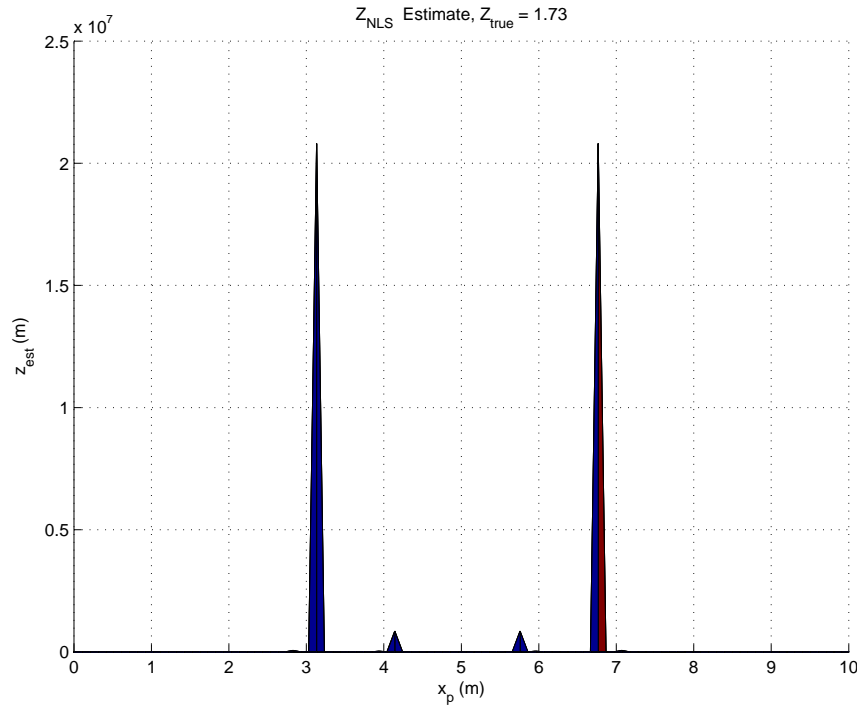


Figure 5.8.: Estimates of z when introducing bias of body boundary in a 10m x 10m room. Plane viewed from the side to show spikes

From the running of the simulations we again see the spikes in height estimate. These are shown in Fig. 5.8. These are not useful estimates, as the real value are 1.74m and the estimates are several km above. This show that the radar setup does not work well for height detection in such a room.

4m x 4m Room

If we try the same setup, but this time in a smaller sized room. The radars are placed in the same manner as the previous simulations, but the locations are now as described in Tab. 5.2. The person are simulated to be of the same height as previously.

From Fig. 5.9 we see that the resulting height estimate in a smaller room the method holds up, but still are deviations. It also show, that the area in the middle of the triangle spanned by the radars have the highest deviations from the true point within

	Radar 1	Radar 2	Radar 3
x	0 m	4 m	2 m
y	0 m	0 m	4 m
z	2.5 m	2.5 m	2.5 m

Table 5.2.: Radar placement in a smaller room

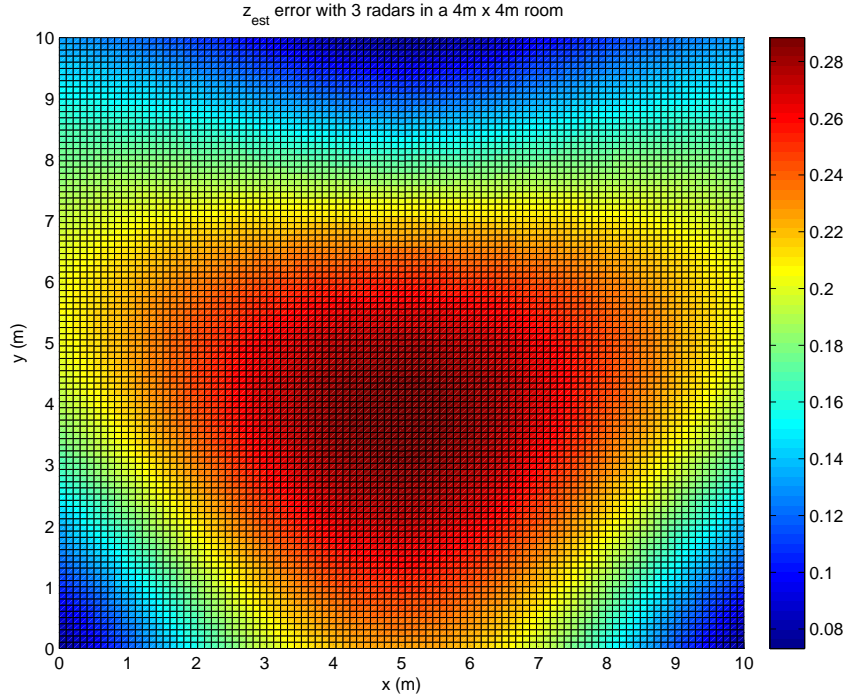


Figure 5.9.: $\hat{z}-z$ when introducing bias of body boundary in a 4m x 4m room.

the sphere. It can be concluded that the area of the triangle spanned by the radar have a significant effect on the height estimate.

We now look at how the height of the sphere affect the measurements. We place the sphere on the floor at the center of the triangle, $(2, 1.48, 0.7)$, and move it up towards the ceiling. By doing so, we find the max height of a person that will still give reasonable height estimates, given the radar arrangement.

We see from Fig. 5.10 that the estimates spikes at around 1.96m. Thus, we have an approximate max height for a room with 4m x 4m area and 2.5 m ceiling height and radars placed accordingly.

5.2.2. 4 Radars

We now introduce a fourth radar to the setup. We will see if the additional radar can solve the bias problem by augmenting the Line of Sight matrix \mathbf{L} with a bias.

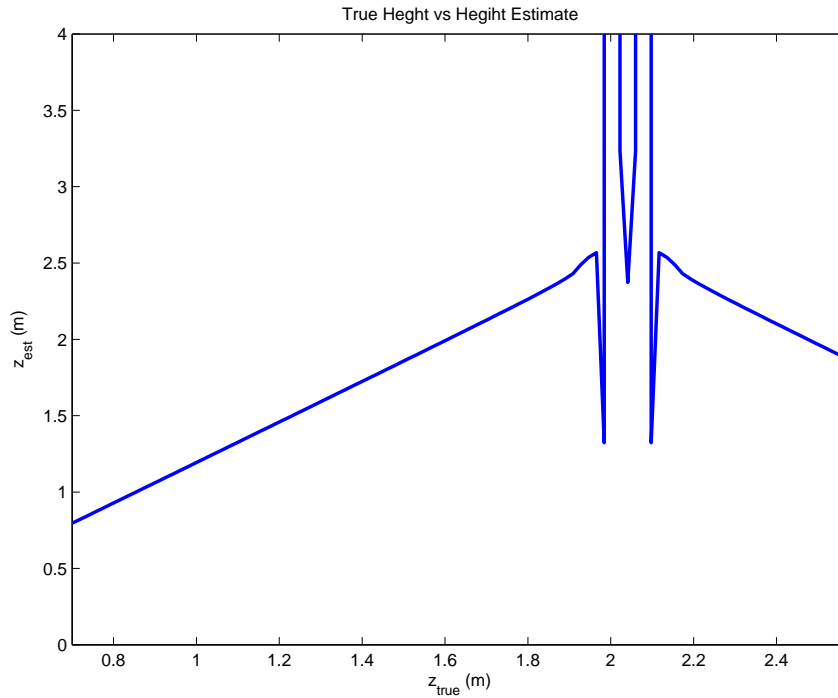


Figure 5.10.: The height estimates as a sphere of radius 0.07m are lifted towards the ceiling.

The placement of the fourth radar should be placed at a location that gives the prism created by the four radars the largest volume, but still be in a location that makes sense. Although the placement giving the largest volume would be in the middle of the floor, this is not a reasonable place to put it. Therefore, the radars are placed in the corners so that the radars construct a coordinate plane along two of the walls and along the ceiling. The placement are shown in Tab. 5.3. The simulations are using the same parameters for the sphere as with the three radar simulations.

	Radar 1	Radar 2	Radar 3	Radar 4
x	0 m	10 m	0 m	0 m
y	0 m	0 m	10 m	0 m
z	2.5 m	2.5 m	2.5 m	0 m

Table 5.3.: Radar placement with four radars

10m x 10m Room

In Fig. 5.11 we see that the simulations show improvement to the height estimation when adding a fourth radar. We saw, that when using three radars that the values spikes in certain locations. Now, we have much more reasonable values, even though the estimates deviates from the real value in the 0m to 0.25 m range.

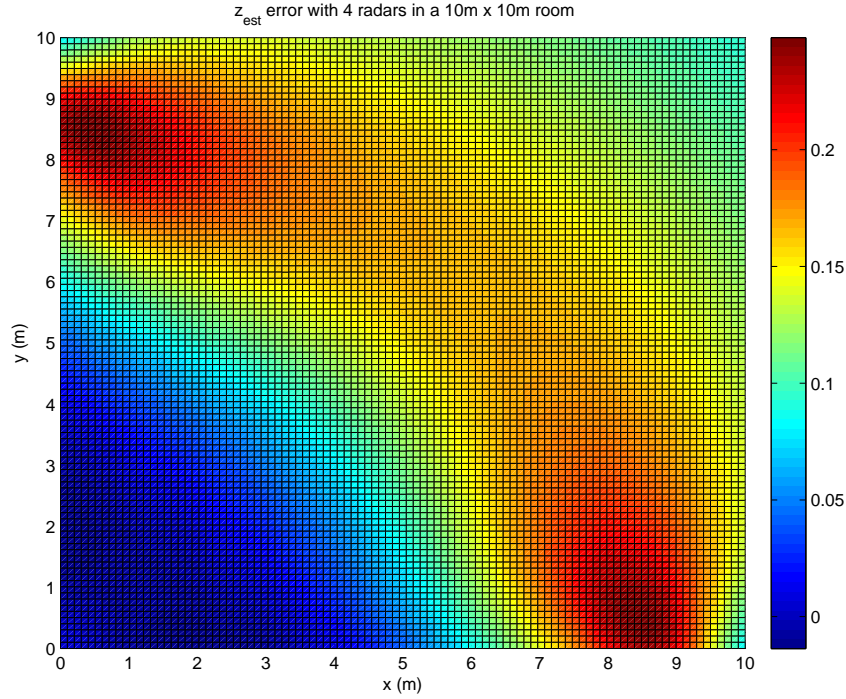


Figure 5.11.: $\hat{z} - z$ when introducing bias of body boundary in a 10m x 10m room

Another observation of interest, is that the Weighted Least Square used as initial estimate to the Nonlinear Least Square are closer to the real value than the outcome of the Nonlinear method. The values are shown in Fig. 5.12.

4m x 4m Room

As in the three radar simulation, we see from Fig. 5.13 improvement to the height estimation are shown when reducing the size of the room. The max deviation are reduced from 0.28m to 0.10m.

Adding β to NLS

If we assume that the bias can be considered to be about the same for all radars, and that the human body is approximately uniform, then we can add the β to the \mathbf{L} matrix and get equation.(3.16). We can now utilize the \mathbf{L}_* matrix in our simulated estimates.

As can be seen in Fig. 5.14, the resulting errors are small enough to be considered zero. However, as the human head is not a perfectly uniform shape, the simulated results are highly idealized.

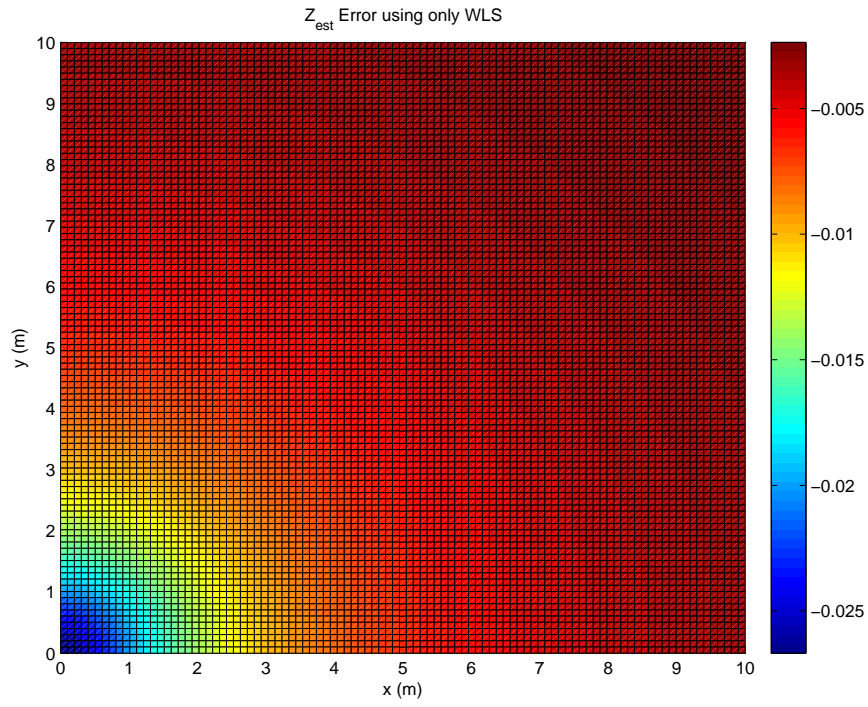


Figure 5.12.: $\hat{z} - z$ when using only the Weighted Least Square method when introducing bias of body boundary in a 10m x 10m room and using four radars.

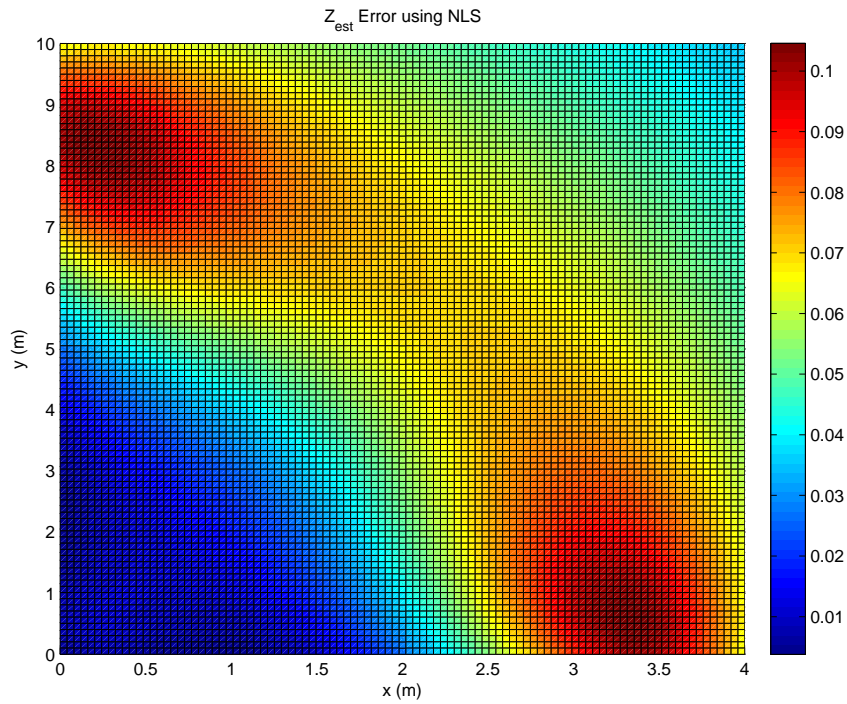


Figure 5.13.: $\hat{z} - z$ when introducing bias of body boundary in a 4m x 4m room.

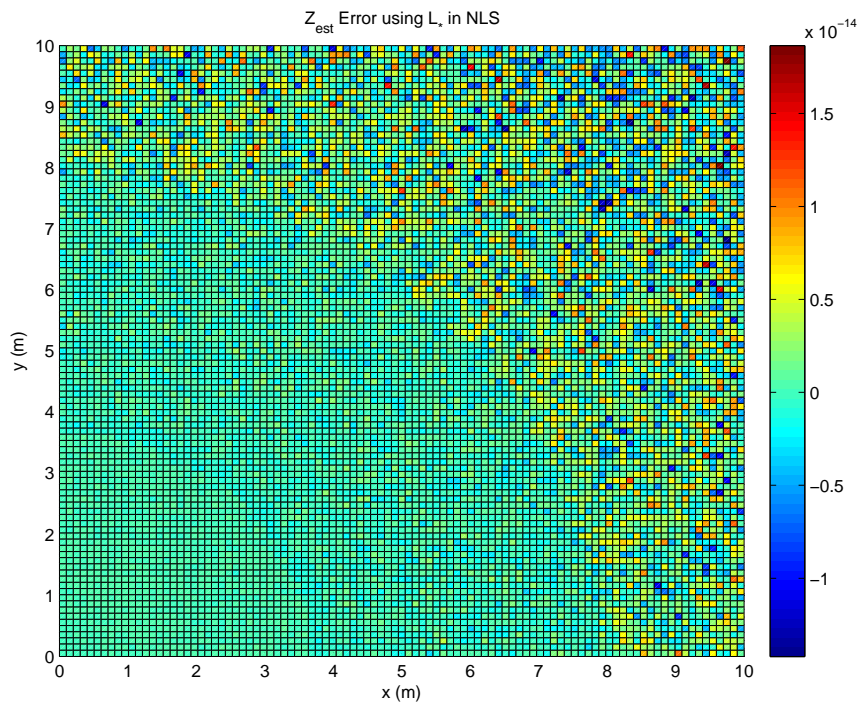


Figure 5.14.: Error in estimate of z when using \mathbf{L}_* to compensate for body boundary in a 10m x 10m room

6. Fall Detection

Based on the now Kalman Filtered estimates, a method for fall detection based on height is proposed and evaluated.

6.1. Height Based Fall Detection

This section will present a method to determine if a person is lying on the floor. It is assumed that we have the observed height, and the height observed the highest location on the body. Therefore, when the estimated height \hat{z} , drops below a chosen threshold, we have an indication for a fall. It is also assumed that a person might want to pick something up from the ground. For this reason, we look at the mean of the height for a period of time before the determining that a fall have occurred. Thus, we suppress possible outliers and we give time to pick objects up from the ground. The steps for this implementation are shown in Algorithm 6.1.

Algorithm 6.1 Height based fall detection algorithm.

```

set           $T_t, T_{\hat{z}}$ 
 $\hat{z}_{\text{stored}}$   = [ ]
while      run
    if           $\text{size}(\hat{z}_{\text{stored}}) < T_t$ 
                 $\hat{z}_{\text{stored}}(\text{end}+1) = \hat{z}$ 
    else
                 $\hat{z}_{\text{stored}} = [\hat{z}_{\text{stored}}(2:\text{end}) \ \hat{z}]$ 
    end
    if           $\text{mean}(\hat{z}_{\text{stored}}) < T_{\hat{z}}$ 
                 $\text{detection} = \text{true};$ 
    end
end

```

The threshold value for height $T_{\hat{z}}$, should be chosen such that height during normal activity should lie above this value. Normal activities could be lying on the couch

or sitting in a chair. T_z is decided to be set to 0.45m above the floor. The value is higher than what is probably the highest point if a person is laying straight out on the floor, but that is not always the case. A person might fall down and have one leg in a position such that the knee is sticking up. The added height chosen to the threshold is to compensate for this possibility. The threshold for how many estimate samples used for averaging should be chosen according to how robust the estimates are. If the measurements are highly fluctuating, even after Kalman Filtering, the number of samples should be large. The larger the number of samples stored also decide how long a person will have to be under the determined height threshold to be detected. Thus, a large window give a longer time for a person to be down on the floor to pick up objects before an alarm goes off.

A simulation of the system are done with 3 radars in a 4m x 4m large room with $z_c = 2.5\text{m}$. The assumptions are as previous simulations from sec. 5.2 where we track a sphere in the room as a model of the human head. In addition, the simulation assumes that the range estimates have white noise added to them in with zero-mean Gaussian distribution and variance $\sigma_r^2 = 10^{-4}$. As we have seen in the earlier simulations, the height estimate deviates the most towards the center of the room. Therefore, to check the robustness we simulate that a person walks straight forward from the middle of one wall towards towards the middle of the room. The fall occurs at $t = 60\text{s}$.

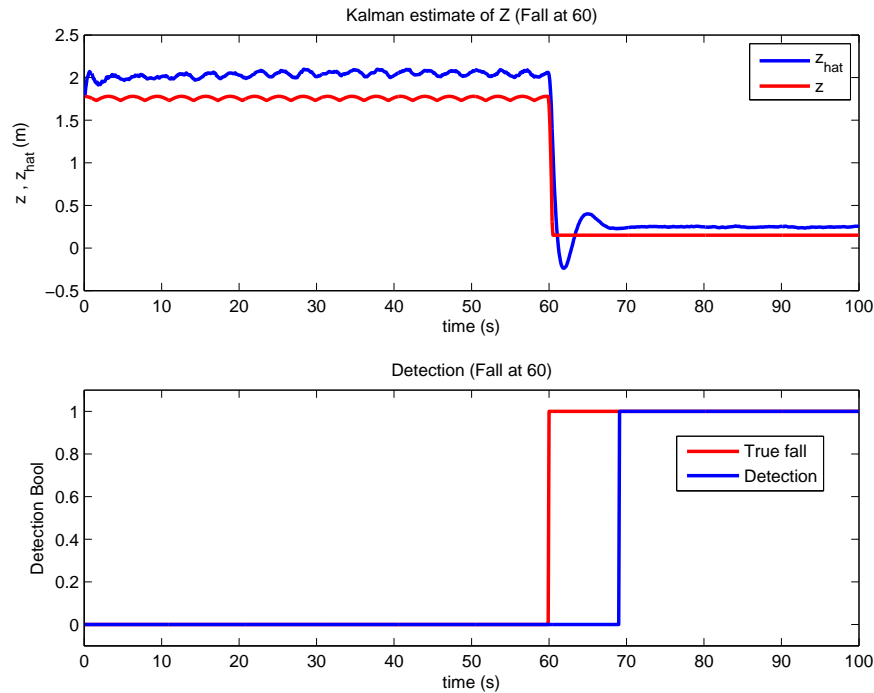


Figure 6.1.: Simulation of a fall in a 4m x 4m room with three radars. Range estimate are effected by white noise with $\sigma_r^2 = 10^{-4}$. The estimates follow the real height and the fall is detected, even with noise added to the range estimates.

As can be seen from Fig. 6.1, the estimate \hat{z} are higher than the real z , but are still sufficiently close enough to detect the fall.

We can now look at how increased noise will effect the estimates. By running the same simulation, but setting the measurement noise variance to $\sigma_r^2 = 0.01$, we can see if the system still are applicable to detect a fall.

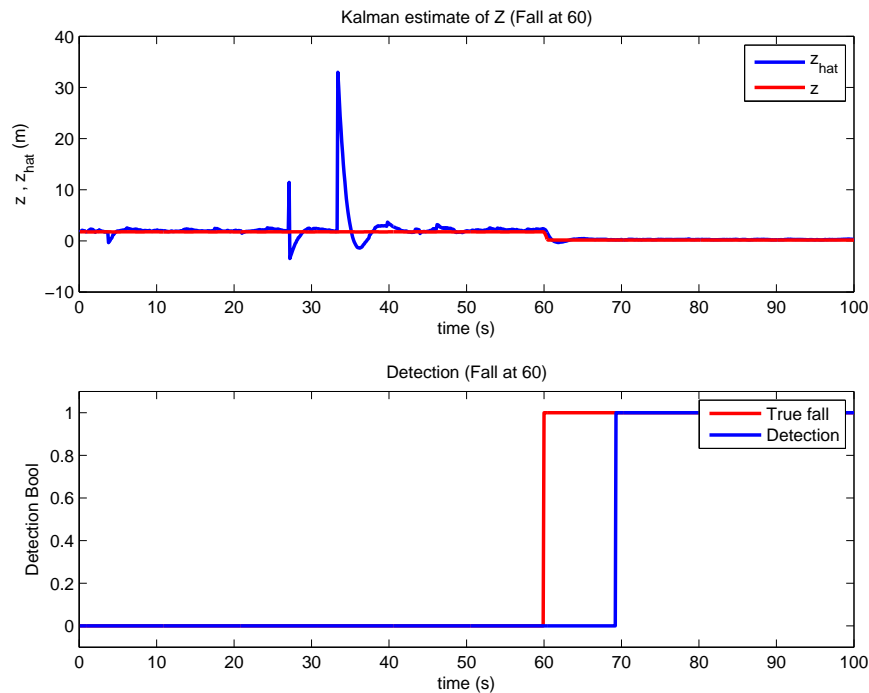


Figure 6.2.: Simulation of a fall in a 4m x 4m room with three radars. Range estimate are effected by white noise with $\sigma_r^2 = 0.01$. The estimates follow the real height and the fall is detected, even with large noise added to the range estimates.

As seen in Fig. 6.2, the estimated heights are sometimes very large or even lower than the floor. The biggest risk here is that the height estimate goes low even when the person is standing. This may give rise to a large number of false detection. Nonetheless, even with large disturbances in the range estimates, the algorithm detects the fall.

A scenario where a person falls but ends up in a sitting position are now simulated. The fall will occur at the same time as previously, but now the height ends up at 0.83m. We assume the measurement variance to be $\sigma_r^2 = 10^{-4}$.

The simulation shows in Fig. 6.3, thatsec. 6.1 the algorithm have shortcomings. It can not be assumed that all falls will end with the person laying flat out on the floor.

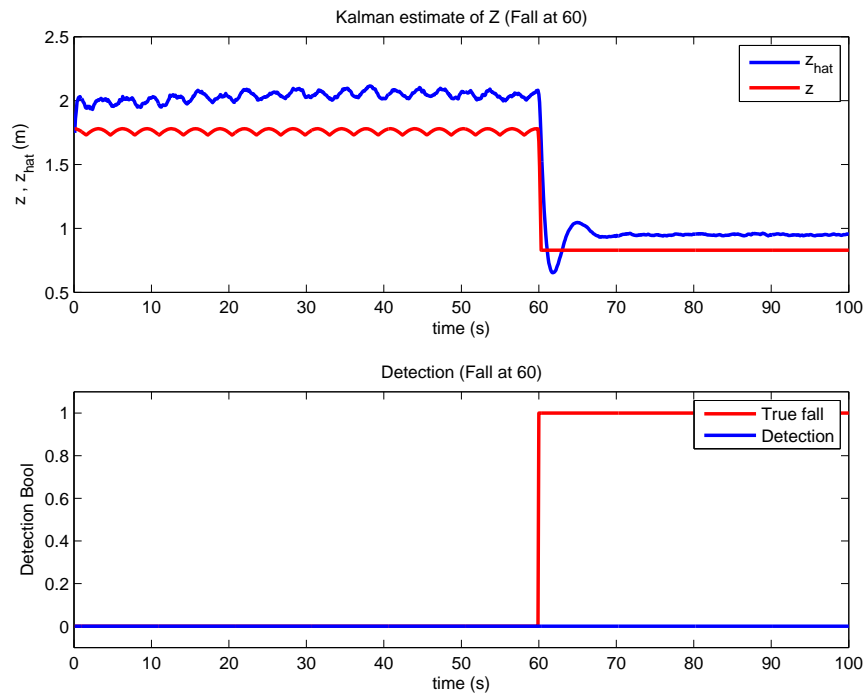


Figure 6.3.: Simulation of a fall in a 4m x 4m room with three radars. Range estimate are effected by white noise with $\sigma_r^2 = 10^{-4}$. The estimates follow the real height and, but the fall is not detected as the height are not below the set threshold.

7. Discussion

In this chapter, the result found in this master thesis will be discussed. Evaluation of the performance of the method for range estimation were conducted in the Project Thesis [3], and a brief evaluation on the added features will be done. We will discuss the methods used to determine the localization by the use of Trilateration and Nonlinear Least Square with Weighted Least Square for initialization in combination with the simulations for localization. The set-up and result from the real test will be evaluated as well as describing the shortcomings the the test itself. Finally, we will discuss the fall-detection algorithm and evaluate the value of the result.

7.1. Ranging

The original range estimation found in the Project Thesis [3], are still applicable within ranges up to 6m. When the distances are larger the reflections are hard to discern from the noise.

7.2. Localization and Tracking

The goal of this thesis is the ability to track a person without the need of any sensory equipment on them. We encounter the problem of finding the position of an object with boundaries, and not a single source. This is a problem when using Trilateration, as it are based of nearly perfect range estimates to a single point. As seen in Fig. 3.3, depending on the location of the object, Trilateration run the risk of not finding a solution. The Nonlinear Least Square method works well to estimate the x and y coordinate when initiated with the Weighted Least Square estimates, but are very reliant on the radar placement to achieve correct estimates of the height. The ceiling was chosen as placement for the radars, as the author wanted to get the most accurate information about the height of the person tracked, as the z coordinate is the most important to determine if a person is standing or lying on the floor. The size of the room and the geometric positioning of the radars also plays a significant role in the accuracy of the methods. The wider the radars are spread apart, the taller the ceiling needs to be, in order for $\hat{\mathbf{x}}$ to be close \mathbf{x} . By placing the radars distributed on the ceiling, the bias problem occurs as long as the person being tracked are located inside the triangle spanned by the radars. Evrendilek and Akcan

[22] presents that the problem with noise and bias in Trilateration is NP-Complete. Since the human body is of a non uniform shape, every radar measurement will introduce a new bias. For every equation we introduce, we also introduce a new unknown.

F. Adib, Z. Kabelax, D. Katabi and R.C. Miller [23] present a very similar setup, but rotated 90 degrees. They place radars in a 'T' shape on a wall, and in this way omits the problem of the body bias. Their measurements are taken from distances varying between 3m and 9m, thus they avoid the problems that arise when the person observed comes close to the radar plane. Given the directionality of the Vivaldi antennas used, their setup would probably be better. Since the Vivaldi antennas are directional, the area where all radars have coverage with their antenna would be larger in a 'T' setup. If omnidirectional antennas were usable the arrangement of radars proposed in this master thesis would be interesting to test. The paper were found at the end of the writing of this thesis, and thus it was not possible to test and reproduce their results.

7.3. Fall Detection

As the fall detection proposed and shown in this thesis are only simulations, it can only give an indication that the system works. As the simulations shown in sec. 6.1, the Kalman estimated states follow the real height within reasonable deviations, even with only three radars present. Since the input of the Kalman Filter is the estimated coordinates from the Nonlinear Least Square method, it is heavily reliant on the size of the room and radar placement.

Given the criteria set for detection is only based on height, the method can detect extreme falls such as 'banana peel fall', where the person are changing from walking to laying on the ground in almost an instant. Given the nature and complexity of possible ways of falling, the author would not characterize it as robust in its current state, nor sufficient, to have as a stand alone home safety system. The low level of information the system have available make it necessary to develop smarter ways to detect if a person have fallen. This might be done by using the history of location where a person usually resides. As an example, a person might use a lot of time in one particular place such as a chair or a sofa.

8. Conclusion

This section cover what this thesis concludes with in regarding the usage of distributed UWB radar for fall detection.

With the use of the radar from Novelda it is possible to generate range estimates to objects within in the spread area of the antennas used. The antennas used in this thesis are Vivaldi antennas, that have a very directional spread. This make them suitable for ranging in a specific direction. But, because of the antennas limited spread, the area covered by all the radars becomes are not as big as desired. When distributed in a room, the area where an object was in the view of all three radars became very limited. Because of this, antennas with a larger spread are desired, preferably omnidirectional.

A problem that became apparent during the work on this thesis, was the problem of a constant bias that give shorter ranges. When a person is located between radars, the ranges estimated are to body's surface. This became a problem when using Trilateration, as the method are reliant on that the measurements coincide at some point. The methods found for localization were dependent on ranges being almost perfect, but with acceptable variances. Little literature were found on the topic of localization with bias giving shorter range estimates.

The thesis focused on that the height of a person observed would be a telling sign to look at for detection of fall. Therefore, it was desired to locate a person in three dimensions. Because of this, at least three radars were needed as we have three unknown. To be able to get the best estimate of the height, the radars were determined to be placed as high in the room as possible. Due to physical limitations, it was not possible to place the radars at the desired heights. The test conducted with the placement of the radars were not able determine a correct three dimensional positioning with the methods found. The test did how ever show that 2D localization were possible even with bias.

Simulations were done with idealized conditions to give an impression on how the methods found in the thesis handled different scenarios. The simulations showed that placement of the radars were important to get reliable height estimates. The wider the radars were spread out, the more sensitive they were to bias. The Line of Sight matrix used in the Nonlinear Least Square method for position estimating, became singular, or close to singular, when an object with volume got near the radar plane. Especially if the object reach the plane in between the radars. But the methods gave acceptable estimates when the radars were closer together, i.e the

rooms were smaller. The simulations are idealized, and there are a lot of possible sources for error in real applications.

The thesis present a method for fall detection by using height as the deciding factor. In simulated scenarios the algorithm detected the fall. The algorithm also held when the estimates were highly unstable. Considering the complexity of real falls, the method alone are not enough. A simulated scenario where a person falls and ends up sitting on the ground were not detected.

9. Future Work

There are a lot of areas to investigate when it comes to the use of ultra wide-band radar for fall detection.

Testing of a real time system with more optimal placement of radars are needed to further verify the findings of this thesis.

The system need verification that the localization method provide correct estimates in a real world testing. For this a video system linked to the radar measurements can be used. VICON is a system that utilizes cameras and markers placed on the body to determine position and posture of the person wearing them.

Stronger combinations of fall detection algorithms needs to be developed should the system be realized for commercial use.

Bibliography

- [1] L. F. Hektoen, E. Aas, and H. Lurås, “Cost-effectiveness in fall prevention for older women,” *Scandinavian journal of public health*, vol. 37, no. 6, pp. 584–589, 2009.
- [2] R. Planinc and M. Kampel, “Introducing the use of depth data for fall detection,” *Personal and ubiquitous computing*, vol. 17, no. 6, pp. 1063–1072, 2013.
- [3] K. Stormo, “Human detection and ranging using uwb radar,” 2013.
- [4] D. Litvak, Y. Zigel, and I. Gannot, “Fall detection of elderly through floor vibrations and sound,” in *Engineering in Medicine and Biology Society, 2008. EMBS 2008. 30th Annual International Conference of the IEEE*, pp. 4632–4635, IEEE, 2008.
- [5] A. Bourke, P. Van de Ven, M. Gamble, R. O’Connor, K. Murphy, E. Bogan, E. McQuade, P. Finucane, G. O’laighin, and J. Nelson, “Evaluation of waist-mounted tri-axial accelerometer based fall-detection algorithms during scripted and continuous unscripted activities,” *Journal of biomechanics*, vol. 43, no. 15, pp. 3051–3057, 2010.
- [6] D. Anderson, J. M. Keller, M. Skubic, X. Chen, and Z. He, “Recognizing falls from silhouettes,” in *Engineering in Medicine and Biology Society, 2006. EMBS’06. 28th Annual International Conference of the IEEE*, pp. 6388–6391, IEEE, 2006.
- [7] S. S. Ghassemzadeh, R. Jana, C. W. Rice, W. Turin, and V. Tarokh, “A statistical path loss model for in-home uwb channels,” in *Ultra Wideband Systems and Technologies, 2002. Digest of Papers. 2002 IEEE Conference on*, pp. 59–64, IEEE, 2002.
- [8] E. K. Jørgensen, “People tracking using short range uwb radars - a basic framework and simulation-based analysis,” 2013.
- [9] O. Wijk, P. Jensfelt, and H. I. Christensen, “Triangulation based fusion of ultrasonic sensor data,” in *Robotics and Automation, 1998. Proceedings. 1998 IEEE International Conference on*, vol. 4, pp. 3419–3424, IEEE, 1998.
- [10] W. Murphy and W. Hereman, “Determination of a position in three dimensions using trilateration and approximate distances,” *Department of Mathematical and Computer Sciences, Colorado School of Mines, Golden, Colorado, MCS-95-07*, vol. 19, 1995.

-
- [11] E. W. Weisstein, "Sphere-sphere intersection, <http://mathworld.wolfram.com/sphere-sphereintersection.html>."
 - [12] M. Mirbach and W. Menzel, "A simple surface estimation algorithm for uwb pulse radars based on trilateration," in *Ultra-Wideband (ICUWB), 2011 IEEE International Conference on*, pp. 273–277, IEEE, 2011.
 - [13] R. B. Thompson, "Global positioning system: the mathematics of gps receivers," *Mathematics magazine*, vol. 71, no. 4, pp. 260–269, 1998.
 - [14] Wikipedia, "<http://en.wikipedia.org/wiki/trilateration>."
 - [15] E. W. Weisstein, "circle-circle intersection, from mathworld—a wolfram web resource. <http://mathworld.wolfram.com/circle-circleintersection.html>."
 - [16] B. Vik, "Integrated satellite and inertial navigation systems," *Department of Engineering Cybernetics, NTNU*, 2009.
 - [17] Y. Chan and K. Ho, "A simple and efficient estimator for hyperbolic location," *Signal Processing, IEEE Transactions on*, vol. 42, no. 8, pp. 1905–1915, 1994.
 - [18] T. I. Fossen, *Handbook of marine craft hydrodynamics and motion control*. John Wiley & Sons, 2011.
 - [19] R. G. Brown, P. Y. Hwang, *et al.*, *Introduction to random signals and applied Kalman filtering*, vol. 3. John Wiley & Sons New York, 1992.
 - [20] S. Zhao, B. M. Chen, and T. H. Lee, "Optimal Sensor Placement for Target Localization and Tracking in 2D and 3D," *ArXiv e-prints*, Oct. 2012.
 - [21] SSB, "Tabell 4.22 vernepliktige etter høyde present."
 - [22] C. Evrendilek and H. Akcan, "On the complexity of trilateration with noisy range measurements," *Communications Letters, IEEE*, vol. 15, no. 10, pp. 1097–1099, 2011.
 - [23] F. Adib, Z. Kabelac, D. Katabi, and R. C. Miller, "3d tracking via body radio reflections," 2013.
 - [24] Novelda, "www.novelda.no," Nov. 2009.

List of Figures

1.1. Data Flow	3
2.1. UWB Pulse Signal	6
2.2. Normalized radar signal represented as a frame.	7
2.3. The signals and values generated by range estimation. Signals have been scaled down and shifted for viewing.	8
3.1. Sphere-Sphere Intersection. Image taken from [11] and [14]	10
3.2. Possible outcomes of z , given arrangement of the (non)intersecting circles. Image taken from [15]	11
3.3. Depending on the location and size of an object, the estimated position from Trilateration can deviate from the real position by a large amount. In both cases the radars are placed in (0,0) and (10,0), and a ball with radius 0.25m are placed at a) (6,1) b) (5,3)	12
3.4. Optimal sensor placement for a given target localization. a) Three sensors for a 2D location. b) Four sensors for a 3D location	19
4.1. Test Setup: The radars annotated with the R1,R2 and R3. The origin of the coordinate system is located below R3. R1 and R2 are placed at a higher level than R3. The mattress on the floor were used to soften the impact of the fall. The PC were located outside the area the radars cover.	24
4.2. Test 1: Walking with fall forward . a) Location estimate from Weighted Least Square. The radar positions are indicated by the points in the center of the circles. The circles are the estimated range for each radar. The red dot outside the circles are the estimate generated by the Least Square method, and the blue dot are the Kalman filtration of this point. b) The Kalman estimated states of z throughout the test. It can be seen that the estimates are centered around zero.	25
4.3. Test 3: Walking with left leg giving in . a) Location estimate from Weighted Least Square. The radar positions are indicated by the points in the center of the circles. The circles are the estimated range for each radar. The red dot outside the circles are the estimate generated by the Least Square method, and the blue dot are the Kalman filtration of this point. b) The Kalman estimated states of z throughout the test. It can be seen that the estimates are centered around zero.	25

4.4. Test 3: Walking with fall to the side . a) Location estimate from Weighted Least Square. The radar positions are indicated by the points in the center of the circles. The circles are the estimated range for each radar. The red dot outside the circles are the estimate generated by the Least Square method, and the blue dot are the Kalman filtration of this point. b) The Kalman estimated states of z throughout the test. It can be seen that the estimates are centered around zero.	26
5.1. Horizontal Movement $z < z_c$: z moves in a parallel plane below the radar plane. True z in the right image. Left image show $z - \hat{z}$	28
5.2. Horizontal Movement $z = z_c$: z moves in the same plane as the radar plane. True z in the right image. Left image show $z - \hat{z}$	29
5.3. Oscillation Movement $z \leq z_c$: z moves in a sinusoidal wave pattern in a plane below the radar plane. True z in the right image. Left image show $z - \hat{z}$	29
5.4. Horizontal Movement $z < z_c$: z moves in a plane below the radar plane. Uniformly distributed noise is added to the range measurements. True z in the right image. Left image show $z - \hat{z}$	30
5.5. Horizontal Movement $z = z_c$: z moves in the same plane as the radars span Uniformly distributed noise is added to the range measurements. True z in the right image. Left image show $z - \hat{z}$	31
5.6. Oscillation Movement $z \leq z_c$: z moves in a wave pattern. Uniformly distributed noise is added to the range measurements. True z in the right image. Left image show $z - \hat{z}$	31
5.7. Illustration of a sphere in a 4m x 4m room with a ceiling height of 2.5m. The black sphere have a radius of 0.07m. The blue radars are placed according to Tab. 5.1.	32
5.8. Estimates of z when introducing bias of body boundary in a 10m x 10m room. Plane viewed from the side to show spikes	33
5.9. $\hat{z}-z$ when introducing bias of body boundary in a 4m x 4m room. . .	34
5.10. The height estimates as a sphere of radius 0.07m are lifted towards the ceiling.	35
5.11. $\hat{z} - z$ when introducing bias of body boundary in a 10m x 10m room	36
5.12. $\hat{z} - z$ when using only the Weighted Least Square method when introducing bias of body boundary in a 10m x 10m room and using four radars.	37
5.13. $\hat{z} - z$ when introducing bias of body boundary in a 4m x 4m room. .	37
5.14. Error in estimate of z when using \mathbf{L}_* to compensate for body boundary in a 10m x 10m room	38

6.1.	Simulation of a fall in a 4m x 4m room with three radars. Range estimate are effected by white noise with $\sigma_r^2 = 10^{-4}$. The estimates follow the real height and the fall is detected, even with noise added to the range estimates.	40
6.2.	Simulation of a fall in a 4m x 4m room with three radars. Range estimate are effected by white noise with $\sigma_r^2 = 0.01$. The estimates follow the real height and the fall is detected, even with large noise added to the range estimates.	41
6.3.	Simulation of a fall in a 4m x 4m room with three radars. Range estimate are effected by white noise with $\sigma_r^2 = 10^{-4}$. The estimates follow the real height and, but the fall is not detected as the height are not below the set threshold.	42
B.1.	Radar Module. Image courtesy Novelda	58
B.2.	NVA6100 Radar Chip. Image courtesy Novelda	58
B.3.	SPI to USB I/O Cable. Image courtesy Novelda	59
B.4.	Vivaldi Antenna. Image courtesy Novelda	59

A. On the CD

The cd contains the matlab scripts and .mat files that are the stored data from the tests conducted.

The file “simulering_fall_NLS” are used to produce the simulation of the falls.

The file “Test_run” are used for replaying the test and uses the method found in this thesis for ranging, estimatin.

A pdf of the thesis is also included.

B. System and Hardware

This appendix lists the specifications of the hardware used in the experiments, the NVA-R641 development kit and Dell Studio 1535 Laptop, and the software used for the processing. Besides the number of radars and the 5m USB cables with amplifier, the rest of the equipment are as used in [3].

Hardware

Novelda Nanoscale Impulse Radar - NVA-R641

The Novelda NVA-R641 is a development kit containing a radar module, with integrated radarchip connected through pins with SPI to USB I/O cable for communication with external controller or PC, and Vivaldi antennas for both receiver and transmitter connected with standard SMA connectors. All information on the radar is gathered from Novelda's homepage [24].

Radar Module

- SPI connection to card
- Grounded coplanar waveguide design
- RF match compatibility option through resistive matching possibility on RX and TX
- 100MHz CXO Oscillator
- On board FLASH
- OTP ID programming option
- Standardized SMA connectors



Figure B.1.: Radar Module. Image courtesy Novelda

Radar Chip

- QFN32, 5x5 mm packaging.
- Single chip CMOS NVA6100 Impulse RADAR
- Transmit bandwidth (-10dB) from 0.85 GHz to 9.55 GHz (nominal)
- Sampling rate > 30GS/s
- 512 simultaneous sampling points.



Figure B.2.: NVA6100 Radar Chip. Image courtesy Novelda

I/O Cable

- USB to SPI I/O bridge from FTDI
- USB 2.0 Hi-Speed (480Mb/s)
- USB power supplied to radar module



Figure B.3.: SPI to USB I/O Cable. Image courtesy Novelda

Novelda Vivaldi Antenna

Frequency: 1.3 GHz - 4.4 GHz

Size: 150mm x 133mm x1.6mm

Azumuth: 40°

Elevation: 100°

Weight: < 55g



Figure B.4.: Vivaldi Antenna. Image courtesy Novelda

Dell Studio 1535 Laptop

The laptop were used for experiments on other location than the office. The small space of the office and moving people, forced test to be conducted at other locations.

The processor is an Intel(R) Mobile Core 2 Duo with each core having a clock speed of 2.50 GHz. Memory installed is 4096MB DDR2 SDRAM and USB 2 Hi-Speed (480Mb/s) ports available.

Software

MATLAB

All programming were done with the numerical computing software MATLAB version R2013a. It has many built in features for easy handling of large vectors or matrices and signal processing. Novelda also supplies MATLAB API for the NVA-641 radar.